

# Rotationally inelastic collisions of excited NaK and NaCs molecules with noble gas and alkali atom perturbers

J. Jones,<sup>1,a)</sup> K. Richter,<sup>1</sup> T. J. Price,<sup>1,b)</sup> A. J. Ross,<sup>2</sup> P. Crozet,<sup>2</sup> C. Faust,<sup>1,c)</sup> R. F. Malenda,<sup>1,d)</sup> S. Carlus,<sup>1</sup> A. P. Hickman,<sup>1</sup> and J. Huennekens<sup>1</sup>

<sup>1</sup>Department of Physics, Lehigh University, 16 Memorial Drive East, Bethlehem, Pennsylvania 18015, USA

<sup>2</sup>Institut Lumière Matière, UMR 5306 Université Lyon I–CNRS, Université de Lyon, 69622 Villeurbanne, France

(Received 25 July 2017; accepted 11 September 2017; published online 11 October 2017)

We report measurements of rate coefficients at  $T \approx 600$  K for rotationally inelastic collisions of NaK molecules in the  $2(A)^1\Sigma^+$  electronic state with helium, argon, and potassium atom perturbers. Several initial rotational levels  $J$  between 14 and 44 were investigated. Collisions involving molecules in low-lying vibrational levels ( $v = 0, 1$ , and  $2$ ) of the  $2(A)^1\Sigma^+$  state were studied using Fourier-transform spectroscopy. Collisions involving molecules in a higher vibrational level,  $v = 16$ , were studied using pump/probe, optical-optical double resonance spectroscopy. In addition, polarization spectroscopy measurements were carried out to study the transfer of orientation in these collisions. Many, but not all, of the measurements were carried out in the “single-collision regime” where more than one collision is unlikely to occur within the lifetime of the excited molecule. The analysis of the experimental data, which is described in detail, includes an estimate of effects of multiple collisions on the reported rate coefficients. The most significant result of these experiments is the observation of a strong propensity for  $\Delta J = \text{even}$  transitions in collisions involving either helium or argon atoms; the propensity is much stronger for helium than for argon. For the initial rotational levels studied experimentally, almost all initial orientation is preserved in collisions of NaK  $2(A)^1\Sigma^+$  molecules with helium. Roughly between  $1/3$  and  $2/3$  of the orientation is preserved in collisions with argon, and almost all orientation is destroyed in collisions with potassium atoms. Complementary measurements on rotationally inelastic collisions of NaCs  $2(A)^1\Sigma^+$  with argon do not show a  $\Delta J = \text{even}$  propensity. The experimental results are compared with new theoretical calculations of collisions of NaK  $2(A)^1\Sigma^+$  with helium and argon. The calculations are in good agreement with the absolute magnitudes of the experimentally determined rate coefficients and accurately reproduce the very strong propensity for  $\Delta J = \text{even}$  transitions in helium collisions and the less strong propensity for  $\Delta J = \text{even}$  transitions in argon collisions. The calculations also show that collisions with helium are less likely to destroy orientation than collisions with argon, in agreement with the experimental results. *Published by AIP Publishing.* <https://doi.org/10.1063/1.4997577>

## I. INTRODUCTION

Rotationally inelastic collisions of homonuclear alkali diatomic molecules with noble gas atom perturbers have attracted a great deal of interest over many years, starting with the pioneering studies of Ottinger *et al.*,<sup>1</sup> Ottinger and Poppe,<sup>2</sup> and Bergmann and Demtröder.<sup>3–5</sup> Brunner *et al.*<sup>6</sup> studied rotationally inelastic collisions of Na<sub>2</sub> ( $A^1\Sigma_u^+$ ) molecules with xenon atoms, while Scott *et al.*<sup>7</sup> studied collisions of Li<sub>2</sub> ( $A^1\Sigma_u^+$ ) molecules with Xe, Ar, and Ne atoms. This latter study was expanded to include vibrationally inelastic collisions and the authors reported a propensity rule

$\Delta J = -4\Delta v$  for the most probable collisional transitions.<sup>8–11</sup> McCaffery provided a theoretical interpretation for this interesting result.<sup>12</sup> Rate coefficients for ro-vibrationally inelastic collisions of Li<sub>2</sub> ( $A^1\Sigma_u^+$ ) molecules with neon atoms were reported by Gao and Stewart<sup>13</sup> and Gao *et al.*,<sup>14</sup> for a wide range of initial vibrational levels, and these results were compared with theoretical calculations obtained using the *ab initio* Li<sub>2</sub> ( $A^1\Sigma_u^+$ ) + Ne potential surface of Ref. 15.

Rotationally inelastic collisions involving heteronuclear alkali diatomic molecules have been much less studied. However, such collisions are of considerable interest since the symmetry of the molecule is broken, thus allowing for the possibility of  $\Delta J = \text{odd}$  as well as  $\Delta J = \text{even}$  collisional transitions ( $J$  is the rotational quantum number). Previously in our group, Wolfe *et al.*<sup>16</sup> carried out a series of measurements to study transfer of population and transfer of orientation in collisions of NaK  $2(A)^1\Sigma^+(v = 16, J = 30)$  molecules with argon and potassium atoms. In that work, Wolfe *et al.* found a strong  $\Delta J = \text{even}$  propensity for collisions with argon, but

<sup>a)</sup>Current address: Physics Department, Gannon University, 109 University Square, Erie, PA 16541, USA.

<sup>b)</sup>Current address: Department of Physics and Astronomy, Purdue University, 525 Northwestern Avenue, West Lafayette, IN 47907, USA.

<sup>c)</sup>Current address: Physics Department, Susquehanna University, 514 University Avenue, Selinsgrove, Pennsylvania 17870, USA.

<sup>d)</sup>Current address: Physics and Earth Science Department, Moravian College, 1200 Main St., Bethlehem, PA 18018, USA.

no such propensity for collisions with potassium. In addition, they found that rotationally inelastic collisions of potassium atoms with NaK  $2(A)^1\Sigma^+(v = 16, J = 30)$  molecules destroy almost all orientation of the molecules, while collisions with argon atoms preserve between roughly 1/3 and 2/3 of the initial orientation.

Theoretical calculations to investigate these collisions have also been undertaken in our group.<sup>17,18</sup> The first efforts addressed collisions of NaK  $2(A)^1\Sigma^+$  with helium because it is a smaller perturber atom. Malenda<sup>17</sup> calculated a preliminary potential energy surface (PES) and carried out quantum mechanical calculations based on the rigid rotor approximation of Arthurs and Dalgarno.<sup>19</sup> These calculations corresponded to  $v = 0$ , included transitions among all rotational states for  $J \leq 20$ , and also provided information about collisional transfer of orientation and alignment. The initial results<sup>17</sup> showed a strong dependence on initial  $J$  for low  $J$  but did not exhibit a propensity for  $\Delta J = \text{even}$  transitions. A subsequent calculation<sup>18</sup> with an improved potential surface did show a  $\Delta J = \text{even}$  propensity although it was less pronounced than observed experimentally. At that point, the source of the discrepancy between the calculations and experiments was not obvious due to differences in the perturber (helium vs. argon), the initial rotational level ( $J \leq 20$  vs.  $J = 30$ ), and the much lower vibrational level ( $v = 0$  vs.  $v = 16$ ) used in the calculations. Two possibilities were that a stronger  $\Delta J = \text{even}$  propensity might only emerge at higher  $v$  and that the propensity might be sensitive to the collision partner.

In light of the interesting possible dependence of the cross sections on initial  $v$  and  $J$ , and in order to provide a more direct comparison to theory, we decided to carry out a new series of measurements to study rotationally inelastic collisions of NaK  $2(A)^1\Sigma^+(v = 16, J = 30)$  molecules with helium perturbers and also to study similar collisions with much lower initial  $v$  and  $J$  for both argon and helium perturbers. Three separate experimental setups were used for these studies. Optical-optical double resonance (OODR) spectroscopy was used at Lehigh University in two configurations: the OODR laser-induced fluorescence (LIF) technique was used to study transfer of population between neighboring rotational levels ( $|\Delta J| \leq 4$ ) in collisions of NaK  $2(A)^1\Sigma^+(v = 16, J = 30)$  molecules with argon, helium, and potassium perturbers, and OODR polarization labeling (PL) spectroscopy was used to study transfer of orientation in rotationally inelastic collisions for the same initial state. Complementary experiments at the Université Lyon I used a Fourier transform spectrometer (FTS) with one-laser LIF to observe long progressions of collisional satellite lines ( $|\Delta J| \leq 64$ ), for NaK in the initial states  $2(A)^1\Sigma^+(v = 0, J = 14)$ , ( $v = 0, J = 30$ ), ( $v = 1, J = 26$ ), and ( $v = 2, J = 44$ ). These studies demonstrate that the  $\Delta J = \text{even}$  propensity is significantly more pronounced for helium collisions than for argon collisions.

As a contrast to the NaK studies, we also carried out a series of measurements at Lehigh of collisions of NaCs  $2(A)^1\Sigma^+(v = 14, J = 32)$  molecules with argon. NaCs has a significantly larger permanent electric dipole moment than NaK, and the difference in mass of sodium and cesium is greater than that of sodium and potassium. Thus the study of rotational

population transfer in NaCs serves as an interesting comparison to similar studies in NaK.

We have also calculated new potential energy surfaces and have carried out large scale coupled-channel scattering calculations for collisions of NaK  $2(A)^1\Sigma^+$  with both helium ( $^1S_0$ ) and argon ( $^1S_0$ ) perturbers, for initial  $J \leq 60$  and  $J \leq 50$ , respectively.<sup>20,21</sup> Most of our scattering calculations<sup>17,18,20,21</sup> invoked the rigid rotor approximation and used only the portion of the PES corresponding to the NaK  $2(A)^1\Sigma^+$  bond length fixed at its equilibrium position. Such calculations best represent vibrationally elastic collisions with  $v = 0$ . Nevertheless, the calculations for several initial values of  $J$  show clear propensities for  $\Delta J = \text{even}$ , which are stronger for helium perturbers than for argon. The calculations also show a dramatic dependence of the transfer of orientation on  $J$  and  $\Delta J$  for  $v = 0$ . Orientation is much more likely to be destroyed in collisions when the initial  $J$  is small, although the details are different for odd and even values of  $\Delta J$ . In order to estimate the effect of vibrational excitation, we carried out a few additional calculations<sup>21</sup> in which we fixed  $v$  at a higher value and averaged the PES's over the NaK bond lengths, using an appropriate vibrational wave function. There is some justification for this approach, which amounts to a coupled-channel expansion that includes ro-vibrational levels for one fixed  $v > 0$ , because measured cross sections for vibrationally inelastic collisions for  $v = 0, 1$ , and 2 are very small.<sup>22</sup> The calculations show that the propensity for  $\Delta J = \text{even}$  transitions has a greater dependence on the perturber than on the initial  $v$ .

The primary purpose of the present paper is to present new experimental results and compare them with theoretical calculations. The details of the calculations will be reported later. This manuscript is organized as follows. Section II presents descriptions of the experimental setups used at Lehigh and in Lyon. Section III discusses the rate equation analysis of the data obtained in the various experiments, and Sec. IV presents the data analysis and fitting. Experimental results and comparison between theory and experiment are presented in Sec. V. Section VI provides a summary of the results and some brief conclusions.

## II. EXPERIMENTAL SETUP

### A. Lehigh setup

The OODR experimental setup is shown schematically in Fig. 1 and is very similar to the setup used by Wolfe *et al.*<sup>16</sup> Briefly, the alkali metal (either a sodium-potassium or a sodium-cesium mixture) is contained in a five-arm crossed heat-pipe oven.<sup>23</sup> The central region of the oven is heated to produce a vapor of alkali atoms (and a small percentage of alkali molecules). Inert buffer gas (either helium or argon) is continuously flowed into the oven through inlets near the ends of the arms, and the valve to the vacuum pump is left slightly open to allow the removal of impurities. Pressure in the oven is continuously monitored using an MKS Baratron capacitance manometer. Cold water is flowed through copper coils to cool the regions near the windows in order to prevent the alkali vapor from reaching the windows. The alkali vapor

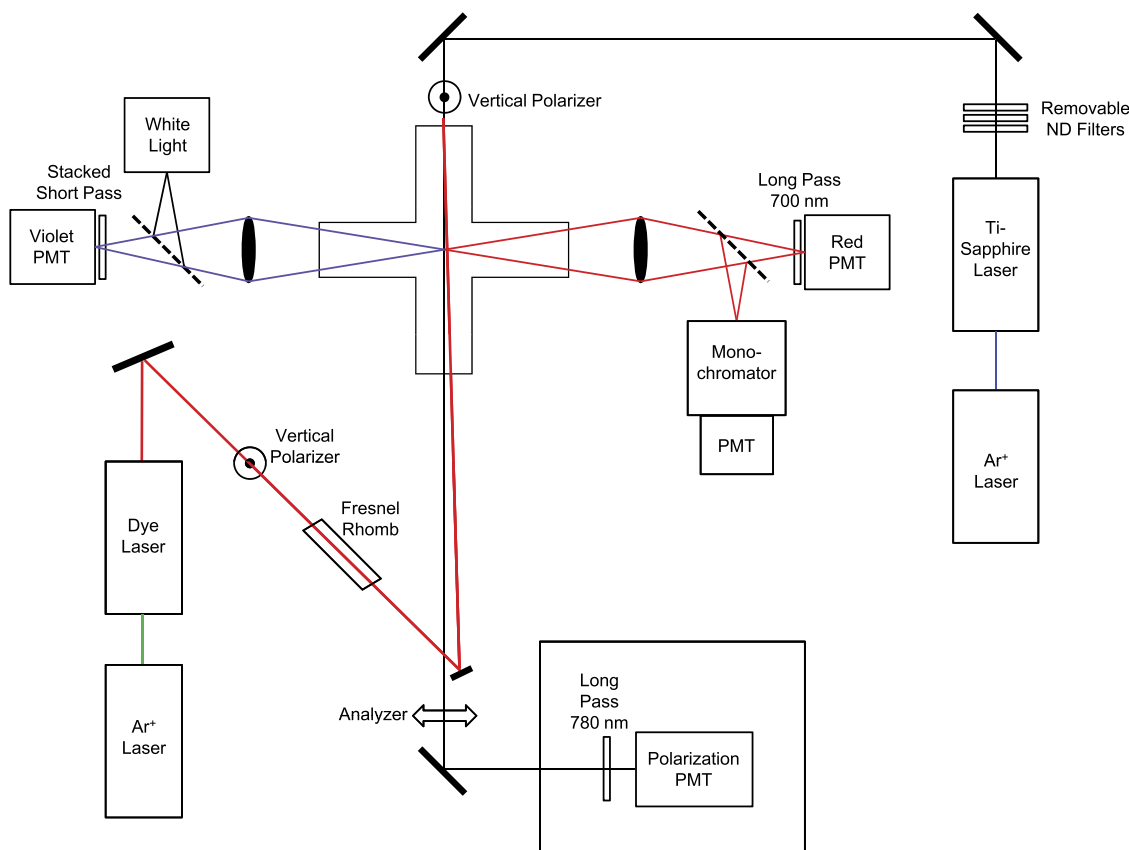


FIG. 1. Experimental setup used at Lehigh University. The white light and monochromator/PMT combination is used in measurements of atomic potassium density using the equivalent width technique. The monochromator (0.33 meter McPherson model 218) was equipped with a 600 groove/mm grating, blazed for  $1 \mu\text{m}$ , and was used in first order. The slits were set to  $50 \mu\text{m}$ , yielding a resolution of  $0.13 \text{ nm}$ .

moves outward from the central region, but encounters the cold buffer gas in the region past the ends of the heaters, and condenses onto the oven walls. A stainless steel mesh lining the oven walls acts as a wick to return the liquid metal back to the hot central region. In the order of decreasing concentration, the oven contains buffer gas atoms (helium or argon), potassium and sodium (or cesium and sodium) atoms, and  $\text{K}_2$ , NaK, and  $\text{Na}_2$  ( $\text{Cs}_2$ , NaCs, and  $\text{Na}_2$ ) molecules.

To obtain the potassium atom density in the NaK experiments, we compared measured white light absorption equivalent widths for the potassium  $D_1$  and  $D_2$  lines (obtained using the monochromator/PMT combination shown in Fig. 1, where PMT stands for photomultiplier tube) to values calculated numerically using the self-broadening rates of Ref. 24 and the noble gas broadening rates of Ref. 25. These white light equivalent width measurements were periodically checked by low-power laser absorption in the far wings of the  $D_1$  line. In the earlier work published by Wolfe *et al.*,<sup>16</sup> the potassium density was determined from the Nesmeyanov vapor pressure formula,<sup>26</sup> corrected downward by 22% since those authors found that the Nesmeyanov formula systematically overestimated the potassium density relative to values obtained with white light absorption. Additional details about the determination of the potassium density can be found in Ref. 16. To determine the noble gas pressure, we first calculated the potassium pressure  $p_K$  from the potassium atom density  $n_K$  using the ideal gas law and subtracted  $p_K$  from the total heat-pipe oven

pressure determined from the capacitance manometer pressure reading. The noble gas atom density was then determined from the noble gas pressure using the ideal gas law.

We used a circularly polarized pump laser (linearly polarized in the case of NaCs) to excite the NaK or NaCs molecules from a particular level of the molecular ground state  $1(X)^1\Sigma^+(v_X, J_X)$  to the  $2(A)^1\Sigma^+$  state level of interest  $2(A)^1\Sigma^+(v, J = J_X \pm 1)$ . The pump laser is either a single-mode cw dye laser (Coherent model 699-29 using LDS 722 dye) for the NaK experiments or a single-mode cw titanium-sapphire (Ti:Sapphire) laser (Coherent model 899-29) for NaCs. Each of these lasers is pumped by an argon ion laser, and each delivers 100-600 mW of power with a line width of  $\sim 1 \text{ MHz}$ . Molecules in the directly excited level  $2(A)^1\Sigma^+(v, J = J_X \pm 1)$  or in the collisionally excited levels  $2(A)^1\Sigma^+(v, J + \Delta J)$  were further excited to levels of the  $3^1\Pi$  state [ $3^1\Pi(v_{3^1\Pi}, J_{3^1\Pi})$ ] for NaK or to levels of the  $5^3\Pi_{\Omega=0}$  state [ $5^3\Pi_{\Omega=0}(v_{5^3\Pi}, J_{5^3\Pi})$ ] for NaCs by a linearly polarized probe laser (Ti:Sapphire for NaK, dye for NaCs). The pump-probe scheme is illustrated in Fig. 2.

For the NaK experiments, we monitored total violet fluorescence from the upper level of the probe transition to the ground state [ $3^1\Pi(v_{3^1\Pi}, J_{3^1\Pi}) \rightarrow 1(X)^1\Sigma^+$  or  $3^1\Pi(v_{3^1\Pi}, J_{3^1\Pi} + \Delta J) \rightarrow 1(X)^1\Sigma^+$ ] as the probe laser frequency was scanned over transitions involving the directly excited level [ $3^1\Pi(v_{3^1\Pi}, J_{3^1\Pi}) \leftarrow 2(A)^1\Sigma^+(v, J)$ ] and over transitions involving the collisionally excited levels [ $3^1\Pi(v_{3^1\Pi},$

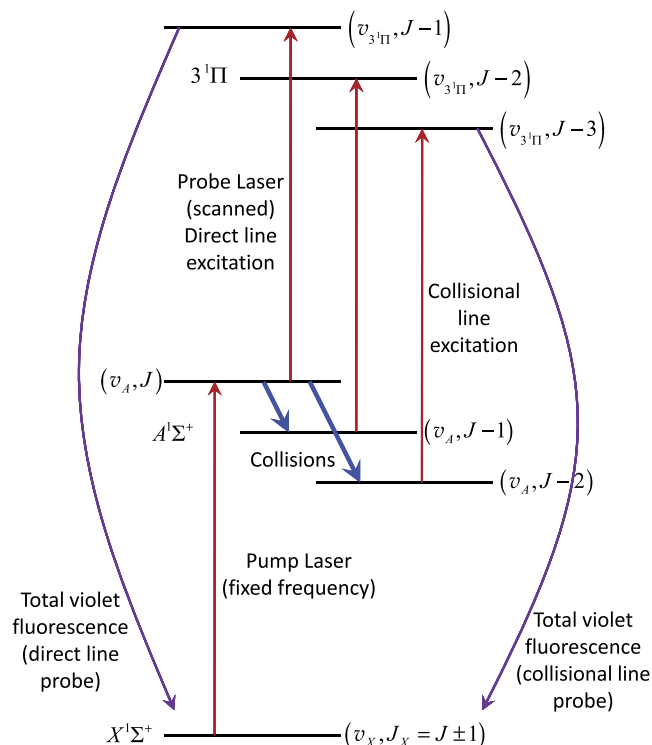


FIG. 2. Energy level diagram for the Lehigh NaK fluorescence experiment. In this example, the frequency of the pump laser is fixed to line center of the  $2(A)^1\Sigma^+(v_A, J) \leftarrow 1(X)^1\Sigma^+(v_X, J_X = J \pm 1)$  transition. The frequency of the probe laser is scanned over the “direct” P line  $3^1\Pi(v_{3^1\Pi}, J-1) \leftarrow 2(A)^1\Sigma^+(v_A, J)$  and over the “collisional” P lines  $3^1\Pi(v_{3^1\Pi}, J-1 + \Delta J) \leftarrow 2(A)^1\Sigma^+(v_A, J + \Delta J)$ . Probe laser excitation is detected by monitoring total violet  $3^1\Pi \rightarrow 1(X)^1\Sigma^+$  fluorescence.

$J_{3^1\Pi} + \Delta J) \leftarrow 2(A)^1\Sigma^+(v, J + \Delta J)$ ]. For NaCs, we monitored green fluorescence from the upper level of the probe transition to the lowest triplet state [ $5^3\Pi_{\Omega=0}(v_{5^3\Pi}, J_{5^3\Pi}) \rightarrow 1(a)^3\Sigma^+$  or  $5^3\Pi_{\Omega=0}(v_{5^3\Pi}, J_{5^3\Pi} + \Delta J) \rightarrow 1(a)^3\Sigma^+$ ] as the probe laser frequency was scanned over transitions involving the directly excited level [ $5^3\Pi_{\Omega=0}(v_{5^3\Pi}, J_{5^3\Pi}) \leftarrow 2(A)^1\Sigma^+(v, J)$ ] and the collisionally excited levels [ $5^3\Pi_{\Omega=0}(v_{5^3\Pi}, J_{5^3\Pi} + \Delta J) \leftarrow 2(A)^1\Sigma^+(v, J + \Delta J)$ ].

The OODR polarization labeling (PL) experiment is designed to study collisional transfer of orientation. Orientation is defined as<sup>27</sup>

$$\mathcal{O} \equiv \frac{\langle M_J \rangle}{\sqrt{J(J+1)}} \quad (1)$$

and hence is non-zero only when the average value of the magnetic quantum number  $M_J$  (projection of  $J$  along the laboratory fixed  $z$ -axis) is non-zero. The setup for the PL experiment is similar to that of the LIF experiment except in the PL experiment the probe laser beam transmitted through the oven passes through a linear polarizer that is (almost) crossed with the probe beam linear polarizer placed before the oven (see Fig. 1). Since the axes of the two linear polarizers are essentially orthogonal, almost no probe laser light passes through the second polarizer, unless the probe beam polarization is altered by the vapor and/or the heat pipe oven windows. The polarization of the probe laser is altered by the vapor when its frequency is tuned to a transition involving one of the levels of the pump

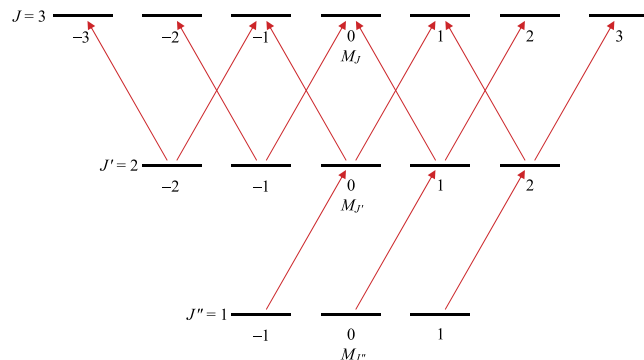


FIG. 3. Energy level (Kastler) diagram showing a circularly polarized pump laser creating an orientation in the intermediate state and a linearly polarized probe laser being used to determine the intermediate state orientation (for purposes of illustration, low values of  $J$  are used in this example). The quantization axis is taken to be the direction of propagation of the pump and probe lasers, and in this coordinate system, the linearly polarized probe can be represented as equal parts of left- and right-circularly polarized light.

transition [in this case, the intermediate level  $2(A)^1\Sigma^+(v, J)$ ]. The circularly polarized pump laser creates an orientation in the upper and lower levels of the pump transition (see Fig. 3). The linearly polarized probe beam can be considered to be composed of equal parts of left- and right-circularly polarized light. However, because the intermediate state  $M_J$  levels are not equally populated (net orientation in the intermediate level), the left- and right-circularly polarized components of the probe beam are not equally absorbed and refracted. Consequently, the transmitted left- and right-circularly polarized components of the probe beam do not sum to pure linearly polarized light upon exiting the oven. Instead, the transmitted probe beam is slightly elliptically polarized and thus some light is transmitted by the second polarizer and enters a photomultiplier tube (labeled polarization PMT in Fig. 1). The directly excited intermediate state level  $2(A)^1\Sigma^+(v, J)$  is oriented by the pump laser and, therefore, large PL signals are observed when the probe laser is tuned to the “direct” probe transition [i.e.,  $3^1\Pi(v_{3^1\Pi}, J_{3^1\Pi}) \leftarrow 2(A)^1\Sigma^+(v, J)$  in NaK]. However, if some fraction of the initial orientation survives a rotationally inelastic collision, then small PL signals can also be observed when the probe beam frequency is tuned to a “collisional” probe transition [i.e.,  $3^1\Pi(v_{3^1\Pi}, J_{3^1\Pi} + \Delta J) \leftarrow 2(A)^1\Sigma^+(v, J + \Delta J)$  in NaK]. We demonstrate in Sec. III that the ratio of collisional to direct line intensities in the PL experiment is directly related to the fraction of orientation that is transferred in the collision.

## B. Lyon setup

The Lyon experiment (see Fig. 4) employs a linear heat pipe oven containing sodium and potassium metals and a fixed amount of noble gas (either helium or argon). In the first group of experiments at Lyon, the buffer gas was introduced into the heat pipe when the oven was cold. The valve was then closed and the oven was heated to the desired temperature. In later experiments, the buffer gas was added or removed when the oven was hot.

Noble gas densities were determined from pressures measured using an MKS capacitance manometer. Potassium

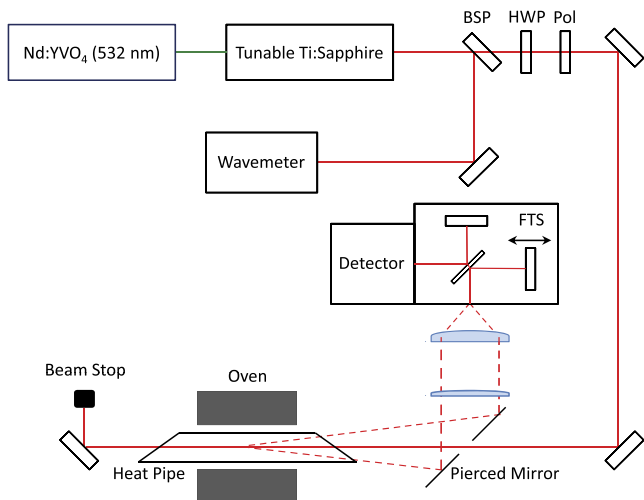


FIG. 4. Experimental setup used at Université Lyon I. The polarizer is set to match the Brewster angle windows on the heat pipe, and the half-wave plate (HWP) allows beam attenuation if necessary. Fluorescence is collected in the backward direction by the pierced mirror and directed to the Fourier transform spectrometer (FTS).

densities were determined from measurements of wavelength-resolved (using the Bomem FTS) white light absorption spectra in the blue wing of the potassium  $D_2$  ( $3S_{1/2} \rightarrow 3P_{3/2}$ ) atomic line, which were compared with calculated absorption line shapes. The absorption line shapes were modeled as Lorentzians since the measurements were taken well outside the Doppler core. The Lorentzian widths were calculated using the potassium self-broadening rates of Ref. 24 and the noble gas broadening rates of Ref. 25.

NaK molecules were excited to a selected level of the  $2(A)^1\Sigma^+$  state [ $2(A)^1\Sigma^+(v, J)$ ], using a single-mode cw Ti:Sapphire laser (Sirah Matisse) pumped by a cw Nd:YVO<sub>4</sub> laser. We chose to populate  $2(A)^1\Sigma^+$  state levels away from known<sup>28</sup> avoided crossings between the  $2(A)^1\Sigma^+$  and  $1(b)^3\Pi$  states, but some rotational levels populated by collisions corresponding to large  $\Delta J$  do not have 100% singlet character (see Sec. V A 4). Fluorescence was collected in the backward direction and sent to the Bomem Fourier transform spectrometer (FTS). Whereas the Lehigh experiment uses the narrow frequency bandwidth of the lasers to separate neighboring rotational lines, the Lyon experiment uses the high resolution of the FTS to accomplish the same thing. The principal advantage of the FTS system, in the present case, is that it allows a large number of collisional satellite lines to be observed and recorded simultaneously. Collisional satellite lines corresponding to  $|\Delta J|$  as large as 64 were observed. In addition, because the direct and collisional satellite line fluorescence is recorded simultaneously, these measurements are not affected by systematic errors such as drift of the laser frequency or laser overlap in the case of OODR.

### III. RATE EQUATION ANALYSIS

#### A. Population transfer

We analyzed the data using a rate equation approach (see Fig. 5). We assume that the pump laser excites a transition

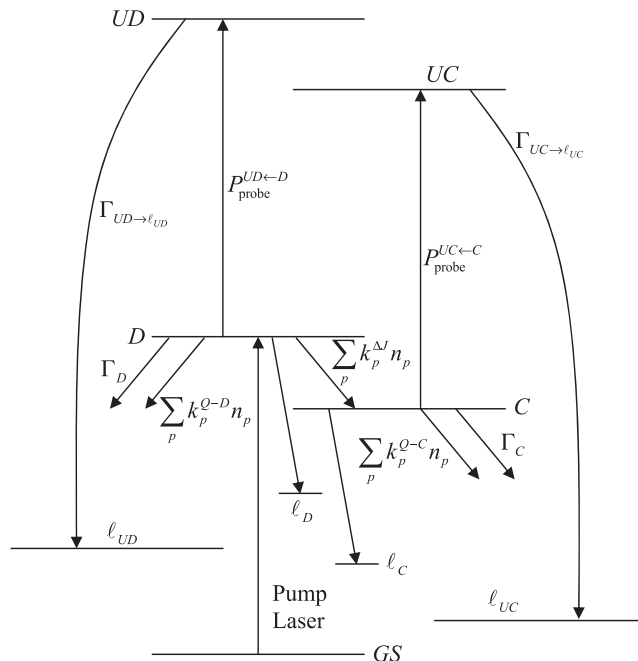


FIG. 5. Schematic diagram showing collisional and radiative population transfer mechanisms included in the rate equation model of Eqs. (2) and (3). Molecules are first excited from the ground state ( $GS$ ) to a specific level  $D$  (for the *Directly* excited level) of the intermediate state using a pump laser whose frequency is fixed to the transition frequency. Collisions take population from the directly excited level  $D$  to a nearby *Collisionally* populated level  $C$ . The probe laser is then used to scan over transitions involving the directly populated and collisionally populated levels to excite the molecules to specific ro-vibrational levels in some upper state,  $UD$  and  $UC$  (for *Upper* level of the probe transition out of level  $D$  and out of level  $C$ , respectively). Levels  $\ell_{UD}$ ,  $\ell_{UC}$ ,  $\ell_D$ , and  $\ell_C$  are lower levels of observed fluorescence channels. See the text for definitions of collisional and radiative rates.

from a particular level of the ground state  $1(X)^1\Sigma^+$ , which we designate  $GS$  in Fig. 5, to a particular level of the  $2(A)^1\Sigma^+$  state, which we designate as level  $D$ . Population in level  $D$  (the directly excited state) is removed in three ways: radiative transitions back to various levels in the ground state  $1(X)^1\Sigma^+$  with a total rate  $\Gamma_D$ , excitation to a level (labeled  $UD$ ) of a higher lying state [ $3^1\Pi$  for NaK or  $5^3\Pi_{\Omega=0}$  for NaCs] by the probe laser at a rate  $P_{\text{probe}}^{UD\leftarrow D}$ , and collisional transitions to other molecular levels at a rate  $\sum_p k_p^{Q-D} n_p$ . Here  $p$  represents the various types of perturbers present in the vapor (“*alk*” denotes alkali atom perturbers and “*NG*” denotes noble gas perturbers),  $n_p$  is the density of perturber  $p$ , and  $k_p^{Q-D}$  is the rate coefficient for all collisions involving perturbers of type  $p$  that transfer population out of level  $D$  to any other final state (quenching collisions). Level  $C$  (the collisional state) is populated by collisions from level  $D$  (or possibly from other nearby levels  $i$ ) at a rate  $\sum_p k_p^{\Delta J} n_p$  ( $\sum_p k_p^{\Delta J_i} n_p$ ) where  $\Delta J = J_C - J_D$  ( $\Delta J_i = J_C - J_i$ ) represents the change in the rotational quantum number between levels  $D$  ( $i$ ) and level  $C$ . Level  $C$  is depopulated by radiative transitions to the ground state at a rate  $\Gamma_C$ , by probe laser excitation at a rate  $P_{\text{probe}}^{UC\leftarrow C}$ , and by quenching collisions at a rate  $\sum_p k_p^{Q-C} n_p$ . If the probe laser intensity is sufficiently high, level  $C$  can also be populated by stimulated emission from the upper level of the probe transition  $UC$  at a rate  $P_{\text{probe}}^{UC\rightarrow C}$  (and

similarly for level  $D$ ). Thus we can write the following steady state rate equation for the population in level  $C$ :

$$\dot{n}_C = 0 = \sum_p k_p^{\Delta J} n_p n_D + \sum_{i \neq D} \sum_p k_p^{\Delta J_i} n_p n_i + P_{\text{probe}}^{UC \rightarrow C} n_{UC} - \left[ \Gamma_C + \sum_p k_p^{Q-C} n_p + P_{\text{probe}}^{UC \leftarrow C} \right] n_C, \quad (2)$$

with solution

$$\begin{aligned} \frac{n_C}{n_D} &= \frac{\sum_p k_p^{\Delta J} n_p + \sum_{i \neq D} \sum_p k_p^{\Delta J_i} n_p \frac{n_i}{n_D}}{\Gamma_C + \sum_p k_p^{Q-C} n_p + P_{\text{probe}}^{UC \leftarrow C} - P_{\text{probe}}^{UC \rightarrow C} \frac{n_{UC}}{n_C}} \\ &= \frac{\sum_p \frac{k_p^{\Delta J}}{\Gamma_C} n_p + \sum_{i \neq D} \sum_p \frac{k_p^{\Delta J_i}}{\Gamma_C} n_p \frac{n_i}{n_D}}{1 + \sum_p \frac{k_p^{Q-C}}{\Gamma_C} n_p + \frac{P_{\text{probe}}^{UC \leftarrow C}}{\Gamma_C} \left( 1 - \frac{g_C}{g_{UC}} \frac{n_{UC}}{n_C} \right)}, \quad (3) \end{aligned}$$

where  $g_i$  is the degeneracy of level  $i$ , and in the last step, we have divided through by  $\Gamma_C$  and used the fact that  $P_{\text{probe}}^{UC \rightarrow C} = \frac{g_C}{g_{UC}} P_{\text{probe}}^{UC \leftarrow C}$ .

Most of the data obtained at Lehigh were collected for  $|\Delta J| \leq 4$  and under ‘‘single collision conditions,’’ where the probability of a rotationally inelastic collision occurring within the excited state lifetime is relatively small, i.e.,  $k_p^{\Delta J} n_p \ll \Gamma_C + \sum_p k_p^{Q-C} n_p$ . Under such conditions,  $\frac{n_i}{n_D} \ll 1$  and

the multi-step collision term  $\sum_{i \neq D} \sum_p \frac{k_p^{\Delta J_i}}{\Gamma_C} n_p \frac{n_i}{n_D}$  in Eq. (3) can be neglected. In Subsection 3 of the Appendix, we discuss data from the Lyon experiment, where collisions involving larger values of  $|\Delta J|$  and higher perturber densities require multiple collision effects to be considered. In the analysis, we also assume that the probe laser intensity is weak (or non-existent as in the Lyon experiment), in which case the term  $P_{\text{probe}}^{UC \leftarrow C}$  can be neglected. Conversely, if the probe laser is strong (saturation limit), the densities of the upper and lower levels of the probe transition are pinned in their statistical ratio and the factor  $\left( 1 - \frac{g_C}{g_{UC}} \frac{n_{UC}}{n_C} \right) \sim 0$ . Finally, we neglect collisions with other alkali diatomic molecules since the molecular densities are small compared with the atomic densities. Thus Eq. (3) reduces to

$$\frac{n_C}{n_D} = \frac{\frac{k_{NG}^{\Delta J}}{\Gamma_C} n_{NG} + \frac{k_{alk}^{\Delta J}}{\Gamma_C} n_{alk}}{1 + \frac{k_{NG}^{Q-C}}{\Gamma_C} n_{NG} + \frac{k_{alk}^{Q-C}}{\Gamma_C} n_{alk}}. \quad (4)$$

### 1. Lyon fluorescence experiment

The analysis of the Lyon one-laser fluorescence experiment is relatively straightforward. In this case, there is no probe laser and population in levels  $D$  and  $C$  is monitored by observing resolved fluorescence on specific transitions  $D \rightarrow \ell_D$  and  $C \rightarrow \ell_C$ , terminating on the ground state levels  $\ell_D$  and  $\ell_C$ , respectively (see Fig. 5). The measured fluorescence intensity for a transition from upper level  $u$  to lower level  $\ell$  is related to the density,  $n_u$ , in the upper level by the following relationship:

$$I = h\nu_{u \rightarrow \ell} n_u V \Gamma_{u \rightarrow \ell} \varepsilon_{u \rightarrow \ell} \frac{d\Omega}{4\pi} F. \quad (5)$$

Here  $h\nu_{u \rightarrow \ell}$  is the photon energy,  $V$  is the observation volume within the oven,  $\Gamma_{u \rightarrow \ell}$  is the radiative rate for the transition (Einstein  $A$  coefficient),  $\varepsilon_{u \rightarrow \ell}$  is the detection system efficiency at the transition frequency,  $\frac{d\Omega}{4\pi}$  is the fraction of the total solid angle subtended by the detector, and  $F$  is an anisotropy factor that accounts for polarization effects and the fact that the emission may not be isotropic. Absolute values for some of these factors are difficult to determine. Therefore, we consider ratios of collisional to direct line fluorescence intensities,

$$\begin{aligned} \frac{I_{C \rightarrow \ell_C}}{I_{D \rightarrow \ell_D}} &= \frac{h\nu_{C \rightarrow \ell_C} n_C V \Gamma_{C \rightarrow \ell_C} \varepsilon_{C \rightarrow \ell_C} \frac{d\Omega}{4\pi} F_{C \rightarrow \ell_C}}{h\nu_{D \rightarrow \ell_D} n_D V \Gamma_{D \rightarrow \ell_D} \varepsilon_{D \rightarrow \ell_D} \frac{d\Omega}{4\pi} F_{D \rightarrow \ell_D}} \\ &= \frac{\nu_{C \rightarrow \ell_C} \Gamma_{C \rightarrow \ell_C} \varepsilon_{C \rightarrow \ell_C} n_C}{\nu_{D \rightarrow \ell_D} \Gamma_{D \rightarrow \ell_D} \varepsilon_{D \rightarrow \ell_D} n_D}, \quad (6) \end{aligned}$$

where in the last step on the right-hand side, we have canceled the terms involving the observation volume, detection solid angle, and anisotropy factors. The last of these is based on the assumption that in both cases, we observe the same type of transition, i.e., P or R line, from the same vibrational band. However, the anisotropy factors may not be strictly equal if the collision partially destroys orientation, since in that case the collisional line is not as strongly polarized as the direct line. Subsection 1 of the Appendix presents a calculation of these  $F$  factors and shows that, for our experiment, the ratio of the anisotropy factors does not differ significantly from unity.

The radiative rates (Einstein  $A$  coefficients) are given by

$$\begin{aligned} \Gamma_{u \rightarrow \ell} = A_{u \rightarrow \ell} &= \frac{8\pi^2 \nu_{u \rightarrow \ell}^3 S_{J_u, J_\ell}}{3\varepsilon_0 c^3 \hbar (2J_u + 1)} \\ &\times \left| \int \chi_u^{v*}(R) \chi_\ell^v(R) dR \int \phi_u^{e*} \hat{\mu}_{e\ell} \phi_\ell^e d^3r \right|^2, \quad (7) \end{aligned}$$

where  $R$  is the internuclear separation of the molecule and  $\vec{r}$  represents all electron coordinates.  $\chi^v$ 's are vibrational wave functions,  $\phi^{e\ell}$ 's are electronic wave functions,  $\hat{\mu}_{e\ell}$  is the electronic dipole moment operator, and  $S_{J_u, J_\ell}$  is the Hönl-London factor. Hence we obtain

$$\begin{aligned} \frac{I_{C \rightarrow \ell_C}}{I_{D \rightarrow \ell_D}} &= \frac{\varepsilon_{C \rightarrow \ell_C} \nu_{C \rightarrow \ell_C}^4 (2J_C + 1)}{\varepsilon_{D \rightarrow \ell_D} \nu_{D \rightarrow \ell_D}^4 (2J_D + 1)} \frac{S_{J_C, J_{\ell_C}}}{S_{J_D, J_{\ell_D}}} \\ &\times \frac{\left| \int \chi_C^{v*} \chi_{\ell_C}^v dR \int \phi_C^{e*} \hat{\mu}_{e\ell} \phi_{\ell_C}^e d^3r \right|^2 n_C}{\left| \int \chi_D^{v*} \chi_{\ell_D}^v dR \int \phi_D^{e*} \hat{\mu}_{e\ell} \phi_{\ell_D}^e d^3r \right|^2 n_D} \quad (8) \end{aligned}$$

for the fluorescence ratio. In this experiment, we observe neighboring rotational lines of the same type (P or R) from the same vibrational band of the same electronic transition. Therefore, the ratio of efficiency factors is approximately one since the detector efficiency does not vary much over the frequency range of these transitions. Additionally, the integrals over the vibrational and electronic wave functions cancel to

good approximation. Consequently, the intensity ratios are given by

$$R_F^{Lyon} \equiv \frac{I_{C \rightarrow \ell_C}}{I_{D \rightarrow \ell_D}} = \frac{v_{C \rightarrow \ell_C}^4 S_{J_C, J_{\ell_C}} (2J_D + 1) n_C}{v_{D \rightarrow \ell_D}^4 S_{J_D, J_{\ell_D}} (2J_C + 1) n_D} = \frac{v_{C \rightarrow \ell_C}^4 S_{J_C, J_{\ell_C}} (2J_D + 1)}{v_{D \rightarrow \ell_D}^4 S_{J_D, J_{\ell_D}} (2J_C + 1)} \left\{ \frac{\frac{k_{NG}^{\Delta J}}{\Gamma_C} n_{NG} + \frac{k_{alk}^{\Delta J}}{\Gamma_C} n_{alk}}{1 + \frac{k_{NG}^{Q-C}}{\Gamma_C} n_{NG} + \frac{k_{alk}^{Q-C}}{\Gamma_C} n_{alk}} \right\}, \quad (9)$$

where the Hönl-London factors for a  $^1\Sigma^+ \rightarrow ^1\Sigma^+$  transition are given by<sup>29</sup>

$$S_{J_u, J_\ell} = \begin{cases} J_u, & \text{for R lines,} \\ J_u + 1, & \text{for P lines.} \end{cases} \quad (10)$$

All of our data correspond to cases where  $J_D \geq 14$ , and for small values of  $|\Delta J|$ , the  $J$  dependent factors are equal to unity to within 2% and can be neglected, especially in comparison to the much larger uncertainties in the alkali atom densities. Similarly, since the collisional and direct lines lie very close in frequency, we could also cancel the frequency factors. In such cases, the measured fluorescence intensity ratios are approximately equal to the density ratio,

$$R_F^{Lyon} \approx \frac{n_C}{n_D} = \frac{\frac{k_{NG}^{\Delta J}}{\Gamma_C} n_{NG} + \frac{k_{alk}^{\Delta J}}{\Gamma_C} n_{alk}}{1 + \frac{k_{NG}^{Q-C}}{\Gamma_C} n_{NG} + \frac{k_{alk}^{Q-C}}{\Gamma_C} n_{alk}}. \quad (11)$$

When larger values of  $|\Delta J|$  are considered, the frequency and  $J$ -dependent terms in Eq. (9) should be retained. Since these terms are easy to include, we analyze all of the Lyon data with Eq. (9).

In many cases, it proved useful to obtain redundant measurements of the same population ratios, especially since some of the collisional lines with large  $|\Delta J|$  are very weak. For example, when we pump level  $2(A)^1\Sigma^+(v=0, J)$ , we determine collisional to direct level population ratios,  $n_C/n_D$ , from both P and R line intensity ratios,  $R_F^{Lyon} = \frac{I_{C \rightarrow \ell_C}}{I_{D \rightarrow \ell_D}}$ , using two separate vibrational bands,  $2(A)^1\Sigma^+(v=0, J) \rightarrow 1(X)^1\Sigma^+(v=9, J \pm 1)$  and  $2(A)^1\Sigma^+(v=0, J) \rightarrow 1(X)^1\Sigma^+(v=10, J \pm 1)$ . Thus, we have four separate measurements of  $n_C/n_D$ . Equation (9) and the approximate equation (11) are valid as long as we only compare P line intensities to P line intensities (and R lines to R lines), and as long as we only compare  $0 \rightarrow 9$  band intensities to  $0 \rightarrow 9$  band intensities ( $0 \rightarrow 10$  band intensities to  $0 \rightarrow 10$  band intensities).

## 2. Lehigh pump-probe experiment

In the Lehigh double-resonance experiment, the direct and collisional level populations are monitored by observing total fluorescence following excitation to an upper state ( $3^1\Pi$  for NaK and  $5^3\Pi_{\Omega=0}$  for NaCs) with the probe laser. Thus in this experiment, the detected fluorescence ratio is given by

$$\frac{I_{UC \rightarrow \ell_{UC}}}{I_{UD \rightarrow \ell_{UD}}} = \frac{\sum_{\ell_{UC}} \epsilon_{UC \rightarrow \ell_{UC}} v_{UC \rightarrow \ell_{UC}}^4 \frac{S_{J_{UC}, J_{\ell_{UC}}}}{(2J_{UC} + 1)}}{\sum_{\ell_{UD}} \epsilon_{UD \rightarrow \ell_{UD}} v_{UD \rightarrow \ell_{UD}}^4 \frac{S_{J_{UD}, J_{\ell_{UD}}}}{(2J_{UD} + 1)}} \times \frac{\left| \int \chi_{UC}^{v*} \chi_{\ell_{UC}}^v dR \int \phi_{UC}^{eI*} \hat{\mu}_{el} \phi_{\ell_{UC}}^{eI} d^3r \right|^2 n_{UC}}{\left| \int \chi_{UD}^{v*} \chi_{\ell_{UD}}^v dR \int \phi_{UD}^{eI*} \hat{\mu}_{el} \phi_{\ell_{UD}}^{eI} d^3r \right|^2 n_{UD}}, \quad (12)$$

where  $UD$  and  $UC$  are the upper state levels of the probe laser transitions out of levels  $D$  and  $C$ , respectively (see Fig. 5), and where the observed fluorescence transitions are described by  $UD \rightarrow \ell_{UD}$  and  $UC \rightarrow \ell_{UC}$ , respectively. We note that  $\ell_{UD}$  and  $\ell_{UC}$  may each represent several lower levels that must be summed over. In the present experiment, the vibrational and electronic wave functions are, to good approximation, identical in levels  $UC$  and  $UD$  and in levels  $\ell_{UC}$  and  $\ell_{UD}$ . Therefore, the integrals over the vibrational and electronic wave functions cancel in the ratio. The Lehigh OODR experiment is limited to  $J_D \geq 14$  and  $|\Delta J| \leq 4$ , so it can be assumed that, as long as the probe transitions are of the same type (i.e., both P, both Q, or both R transitions), the efficiency and frequency factors are close to unity. For the NaK experiment, we observe violet  $3^1\Pi \rightarrow 1(X)^1\Sigma^+$  fluorescence. So the Hönl-London factors  $S_{J_{UC}, J_{\ell_{UC}}}$  are either the sum of the P and R line factors or the Q line factor by itself, depending on whether a P or R line probe transition or a Q line probe transition is chosen. In either case, the Hönl-London factors yield

$$S_{J_{UC}, J_{\ell_{UC}}} = \frac{(2J_{UC} + 1)}{4}, \quad (13)$$

and the  $J$  dependent factors cancel. Thus we find that

$$\frac{I_{UC \rightarrow \ell_{UC}}}{I_{UD \rightarrow \ell_{UD}}} \approx \frac{n_{UC}}{n_{UD}}. \quad (14)$$

The Hönl-London factors are more complicated in the case of the transitions involved in the NaCs experiments, but we take Eq. (14) to be valid in that case as well.

To determine the population ratio  $n_{UC}/n_{UD}$ , we develop the following steady-state rate equation model for level  $UC$ :

$$\dot{n}_{UC} = 0 = P_{\text{probe}}^{UC \leftarrow C} n_C - \left( \Gamma_{UC} + k_{NG}^{Q-UC} n_{NG} + k_{alk}^{Q-UC} n_{alk} + P_{\text{probe}}^{UC \rightarrow C} \right) n_{UC}, \quad (15)$$

which yields the solution

$$n_{UC} = n_C \frac{P_{\text{probe}}^{UC \leftarrow C}}{\left( \Gamma_{UC} + k_{NG}^{Q-UC} n_{NG} + k_{alk}^{Q-UC} n_{alk} + \frac{g_C}{g_{UC}} P_{\text{probe}}^{UC \leftarrow C} \right)}, \quad (16)$$

and similarly for level  $UD$ . We note that the  $P_{\text{probe}}^{UC \leftarrow C}$  term in the numerator represents absorption on the probe transition, while the  $P_{\text{probe}}^{UC \leftarrow C}$  term in the denominator represents stimulated emission. If  $P_{\text{probe}}^{UC \leftarrow C} \gg \Gamma_{UC} + k_{NG}^{Q-UC} n_{NG} + k_{alk}^{Q-UC} n_{alk}$  (i.e., in the saturation limit), we find

$$\frac{n_{UC}}{n_C} = \frac{g_{UC}}{g_C} = \frac{2J_{UC} + 1}{2J_C + 1}, \quad (17)$$

while in the opposite (weak probe) limit,  $P_{\text{probe}}^{UC \leftarrow C} \ll \Gamma_{UC} + k_{NG}^{Q-UC} n_{NG} + k_{alk}^{Q-UC} n_{alk}$ ,

$$\frac{n_{UC}}{n_C} = \frac{P_{\text{probe}}^{UC \leftarrow C}}{\left(\Gamma_{UC} + k_{NG}^{Q-UC} n_{NG} + k_{alk}^{Q-UC} n_{alk}\right)}. \quad (18)$$

By substituting Eqs. (17) and (18) (and similar expressions for  $n_{UD}/n_D$ ) into Eq. (14), we obtain the following expressions for the observed collisional to direct line fluorescence intensity ratios in terms of the collisional and direct level population ratio:

$$\frac{I_{UC \rightarrow \ell_{UC}}}{I_{UD \rightarrow \ell_{UD}}} \approx \frac{n_C}{n_D} \left( \frac{2J_{UC} + 1}{2J_{UD} + 1} \right) \left( \frac{2J_D + 1}{2J_C + 1} \right) \quad (\text{saturation limit}) \quad (19)$$

and

$$\begin{aligned} \frac{I_{UC \rightarrow \ell_{UC}}}{I_{UD \rightarrow \ell_{UD}}} &= \frac{n_C}{n_D} \left( \frac{2J_{UC} + 1}{2J_{UD} + 1} \right) \left( \frac{2J_D + 1}{2J_C + 1} \right) \frac{P_{\text{probe}}^{UC \leftarrow C}}{P_{\text{probe}}^{UD \leftarrow D}} \\ &\times \left\{ \frac{\Gamma_{UD} + k_{NG}^{Q-UD} n_{NG} + k_{alk}^{Q-UD} n_{alk}}{\Gamma_{UC} + k_{NG}^{Q-UC} n_{NG} + k_{alk}^{Q-UC} n_{alk}} \right\} \\ &(\text{weak probe limit}). \end{aligned} \quad (20)$$

The factor  $\left(\frac{2J_{UC}+1}{2J_{UD}+1}\right)\left(\frac{2J_D+1}{2J_C+1}\right)$  is always very close to unity for our experimental conditions. The probe pumping rates are proportional to the probe laser intensity multiplied by the Einstein  $B$  coefficients, which are in turn proportional to the Einstein  $A$  coefficients divided by  $\nu^3$ . Therefore, assuming that the probe intensity is the same when probing levels  $C$  and  $D$ , we find

where for the probe transitions

$$\begin{aligned} S_{J_{UC}, J_C} &= \frac{1}{4} \begin{cases} J_{UC} + 1 \\ 2J_{UC} + 1 \\ J_{UC} \end{cases} \\ &= \frac{1}{4} \begin{cases} J_C + 2 & \text{for R probe transition,} \\ 2J_C + 1 & \text{for Q probe transition,} \\ J_C - 1 & \text{for P probe transition} \end{cases} \end{aligned} \quad (22)$$

and similarly for  $S_{J_{UD}, J_D}$ . Thus we also find that  $P_{\text{probe}}^{UC}/P_{\text{probe}}^{UD} \sim 1$  to a very good approximation. Since levels  $UC$  and  $UD$  are nearby levels of the same vibrational and electronic states, we also assume that they have nearly the same quenching rates and same radiative rates. Then the factor in braces in Eq. (20) cancels and, consequently,

$$R_F^{\text{Lehigh}} \equiv \frac{I_{UC \rightarrow \ell_{UC}}}{I_{UD \rightarrow \ell_{UD}}} = \frac{n_C}{n_D} = \frac{\frac{k_{NG}^{\Delta J} n_{NG} + k_{alk}^{\Delta J} n_{alk}}{\Gamma_C}}{1 + \frac{k_{NG}^{Q-C}}{\Gamma_C} n_{NG} + \frac{k_{alk}^{Q-C}}{\Gamma_C} n_{alk}} \quad (23)$$

is valid to within a few percent, in either the weak probe or strong probe regime. However, for intermediate intensities such that  $P_{\text{probe}}^{UC \leftarrow C} \sim \Gamma_{UC} + k_{NG}^{Q-UC} n_{NG} + k_{alk}^{Q-UC} n_{alk}$ , one should go back and insert Eq. (3) into the rate equation (15), which yields

$$\begin{aligned} R_F^{\text{Lehigh}} &= \frac{n_{UC}}{n_{UD}} = \frac{P_{\text{probe}}^{UC \leftarrow C} \left( \Gamma_{UD} + k_{NG}^{Q-UD} n_{NG} + k_{alk}^{Q-UD} n_{alk} + \frac{g_D}{g_{UD}} P_{\text{probe}}^{UD \leftarrow D} \right) n_C}{P_{\text{probe}}^{UD \leftarrow D} \left( \Gamma_{UC} + k_{NG}^{Q-UC} n_{NG} + k_{alk}^{Q-UC} n_{alk} + \frac{g_C}{g_{UC}} P_{\text{probe}}^{UC \leftarrow C} \right) n_D} \\ &\approx \frac{n_C}{n_D} = \frac{\frac{k_{NG}^{\Delta J} n_{NG} + k_{alk}^{\Delta J} n_{alk}}{\Gamma_C}}{1 + \frac{k_{NG}^{Q-C}}{\Gamma_C} n_{NG} + \frac{k_{alk}^{Q-C}}{\Gamma_C} n_{alk} + \frac{P_{\text{probe}}^{UC \leftarrow C}}{\Gamma_C} \left( 1 - \frac{g_C}{g_{UC}} \frac{n_{UC}}{n_C} \right)}. \end{aligned} \quad (24)$$

Nevertheless, for the probe laser intensities used in the present work, we assume that Eq. (23) is valid.

In general, we use the more exact expression (9) to analyze the Lyon fluorescence data because we have observed large values of  $\Delta J$  in that experiment ( $|\Delta J| \leq 64$ ). We use Eq. (23) to analyze the Lehigh OODR fluorescence data, which are limited to  $|\Delta J| \leq 4$ .

## B. Orientation transfer

Wolfe *et al.*<sup>16</sup> showed that, for a circularly polarized pump and linearly polarized probe, the transmitted probe beam intensity in the polarization spectroscopy experiment could be represented by their Eq. (15), which can be rewritten as

$$\begin{aligned} I_t &= I_0 e^{-2(\beta+\alpha)} \left\{ \xi + (\theta')^2 + \Delta\beta^2 \right. \\ &\quad \left. + (2\Delta\beta + \Delta\alpha_0) \frac{\Delta\alpha_0}{1+x^2} + 2\theta' \frac{\Delta\alpha_0 x}{1+x^2} \right\} \end{aligned} \quad (25)$$

(see also Ref. 30). In this expression, we consider the linearly polarized probe laser to consist of equal parts of left- and right-circularly polarized light at the entrance to the oven and we write the complex refractive indices for left (+) or right (−) circularly polarized light for the oven windows and for the vapor as  $n_w^\pm = \text{Re}[n_w^\pm] + i \text{Im}[n_w^\pm]$  and  $n_v^\pm = \text{Re}[n_v^\pm] + i \text{Im}[n_v^\pm]$ , respectively. With  $\omega$ ,  $c$ ,  $d$ , and  $L$  being the frequency, speed of light in vacuum, window thickness, and length of the vapor column, respectively, we define  $n \equiv (L\omega/2c) \text{Re}[n_v^+ + n_v^-]$ ,  $\Delta n \equiv (L\omega/2c) \text{Re}[n_v^+ - n_v^-]$ ,  $\alpha \equiv (L\omega/2c) \text{Im}[n_v^+ + n_v^-]$ ,  $\Delta\alpha \equiv (L\omega/2c) \text{Im}[n_v^+ - n_v^-]$ ,  $b \equiv (d\omega/c) \text{Re}[n_w^+ + n_w^-]$ ,  $\Delta b \equiv (d\omega/c) \text{Re}[n_w^+ - n_w^-]$ ,  $\beta \equiv (d\omega/c) \text{Im}[n_w^+ + n_w^-]$ , and  $\Delta\beta \equiv (d\omega/c) \text{Im}[n_w^+ - n_w^-]$ . The complex index of refraction of the vapor is frequency dependent and obeys the dispersion relation of Kronig and Kramers:  $\Delta\alpha(\omega) = \Delta\alpha_0/(1+x^2)$ ,  $\Delta n(\omega) = \Delta\alpha_0 x/(1+x^2)$ , where  $x \equiv 2(\omega_0 - \omega)/\Gamma$  is the normalized frequency detuning from line center and where  $\Delta\alpha_0$  is the circular dichroism at line center.<sup>30</sup> The factor  $\xi$  is the extinction

ratio of the polarizer pair (i.e., the transmission of the “wrong” polarization when the polarizers are perfectly crossed),  $\theta$  is the uncrossing angle of the two polarizers, and  $\theta' \equiv \theta + \Delta b$ . The first three terms inside the braces of Eq. (25), which can be measured term by term,<sup>31</sup> do not depend strongly on frequency and therefore only contribute to the background as the probe laser is scanned over resonance. The last term in Eq. (25), proportional to  $x/(1+x^2)$ , gives rise to dispersion shaped signals and can be eliminated by adjusting the uncrossing angle to make  $\theta' \approx 0$ .

The remaining frequency dependent term in Eq. (25) is Lorentzian in shape. In most cases,  $2\Delta\beta \gg \Delta\alpha_0$ . Therefore, the measured intensity at line center in the polarization spectroscopy experiment is proportional to the difference in absorption of the left- and right-circularly polarized components of the probe beam. Wolfe *et al.*<sup>16</sup> showed that the line intensity corresponding to the probe “direct line” transition  $D \rightarrow UD$  could be written as

$$I_{pol}^{D \rightarrow UD} \propto f(J_{UD}, J_D) \langle M_{J_D} \rangle n_D \quad (26)$$

and similarly for the “collisional line” transition  $C \rightarrow UC$ . The factors  $f(J, J')$  are defined in Table I of Ref. 16. Using the definition of orientation,  $\mathcal{O}$ , in Eq. (1), we find that the ratio of collisional line to direct line intensities in the polarization experiment is given by

$$\begin{aligned} \frac{I_{pol}^{C \rightarrow UC}}{I_{pol}^{D \rightarrow UD}} &= \frac{f(J_{UC}, J_C) \langle M_{J_C} \rangle n_C}{f(J_{UD}, J_D) \langle M_{J_D} \rangle n_D} \\ &= \frac{f(J_{UC}, J_C) \sqrt{J_C(J_C+1)} \mathcal{O}_C n_C}{f(J_{UD}, J_D) \sqrt{J_D(J_D+1)} \mathcal{O}_D n_D}. \end{aligned} \quad (27)$$

We note that the  $\sqrt{J(J+1)}$  factors were not included in the definition of orientation given by Wolfe *et al.* Thus, the factors describing the fraction of orientation preserved in a collision  $(1 - f_p^{\Delta J})$  reported by Wolfe should be multiplied by  $\sqrt{J_D(J_D+1)}/\sqrt{J_C(J_C+1)}$  for comparison to the values reported here [see Eq. (27) in the work of Wolfe and Eq. (32) below].

Wolfe *et al.* used a rate equation analysis to describe the product of steady-state orientation and population in the collisional level  $C$ . Following Wolfe, but including the  $\sqrt{J(J+1)}$  factors, we write

$$\begin{aligned} \frac{d}{dt} (\mathcal{O}_C n_C) &= 0 = \left[ k_{NG}^{\mathcal{O}, \Delta J} n_{NG} + k_{alk}^{\mathcal{O}, \Delta J} n_{alk} \right] \mathcal{O}_D n_D \\ &\quad - \left[ \Gamma_C + g_{NG}^C n_{NG} + g_{alk}^C n_{alk} \right] \mathcal{O}_C n_C \end{aligned} \quad (28)$$

with solution

$$\frac{\mathcal{O}_C n_C}{\mathcal{O}_D n_D} = \frac{\frac{k_{NG}^{\mathcal{O}, \Delta J}}{\Gamma_C} n_{NG} + \frac{k_{alk}^{\mathcal{O}, \Delta J}}{\Gamma_C} n_{alk}}{1 + \frac{g_{NG}^C}{\Gamma_C} n_{NG} + \frac{g_{alk}^C}{\Gamma_C} n_{alk}}. \quad (29)$$

In this expression, the rate coefficients for collisional transfer of orientation times population,  $k_p^{\mathcal{O}, \Delta J}$ , can be written as a product of the rate coefficient for transfer of population,  $k_p^{\Delta J}$ , and the fraction of orientation that is preserved in the  $J$ -changing collision,  $(1 - f_p^{\Delta J})$ . The factor  $f_p^{\Delta J}$  [which is not to be confused with  $f(J, J')$  factors above] is defined to be the fraction of orientation that is lost in a collision with species  $p$  that

transfers population from level  $D$  to level  $C$  characterized by  $\Delta J$ . Thus,

$$k_p^{\mathcal{O}, \Delta J} = k_p^{\Delta J} (1 - f_p^{\Delta J}). \quad (30)$$

The  $g_p^C$  factors in Eq. (29) are the rate coefficients for total collisional destruction of population or orientation of molecules in level  $C$ , which can be written as

$$g_p^C = k_p^{Q-C} + g'_p, \quad (31)$$

where  $k_p^{Q-C}$  is the rate coefficient for total collisional quenching (loss of population) of level  $C$  due to collisions with species  $p$ , while  $g'_p$  represents the rate coefficient for decay of orientation in collisions of molecules in level  $C$  with species  $p$  that do not result in a change of  $J$ . By inserting Eqs. (29)–(31) into Eq. (27), we obtain the final expression for the intensity ratio,  $R_P$ , in the polarization spectroscopy experiment,

$$\begin{aligned} R_P \equiv \frac{I_{pol}^{C \rightarrow UC}}{I_{pol}^{D \rightarrow UD}} &= \frac{f(J_{UC}, J_C) \sqrt{J_C(J_C+1)}}{f(J_{UD}, J_D) \sqrt{J_D(J_D+1)}} \\ &\times \left\{ \frac{\frac{k_{NG}^{\Delta J}}{\Gamma_C} (1 - f_{NG}^{\Delta J}) n_{NG} + \frac{k_{alk}^{\Delta J}}{\Gamma_C} (1 - f_{alk}^{\Delta J}) n_{alk}}{1 + \left( \frac{k_{NG}^{Q-C}}{\Gamma_C} + \frac{g'_{NG}}{\Gamma_C} \right) n_{NG} + \left( \frac{k_{alk}^{Q-C}}{\Gamma_C} + \frac{g'_{alk}}{\Gamma_C} \right) n_{alk}} \right\}. \end{aligned} \quad (32)$$

This expression was used to analyze the Lehigh polarization spectroscopy data.

### C. Uncertainties

The major sources of uncertainty in our measured rate coefficients for population transfer and probabilities for destruction of orientation are the uncertainties in the determination of the potassium and noble gas densities.

The uncertainty in the potassium density is particularly large because the heat pipe oven is far from an ideal environment for determining atomic densities. Wolfe *et al.*<sup>16</sup> provide a lengthy discussion of the determination of potassium density in the Lehigh experiments. In the experiments of Ref. 16, the potassium density,  $n_K$ , was obtained from the Nesmeyanov vapor pressure formula corrected by white-light absorption equivalent width measurements on the  $D_1$  and  $D_2$  lines of potassium. In the more recent Lehigh experiments included here, the density was usually determined by equivalent width measurements, which were compared with model calculations. These were periodically checked by low-power laser absorption in the red wing of the potassium  $D_1$  line. In Lyon, the potassium density was determined using wavelength dependent white-light absorption at several chosen frequencies in the blue wing of the  $D_2$  line, using the Bomem FTS to provide the wavelength resolution. In all cases, we assign uncertainties of 30% to the potassium density determinations, consistent with earlier studies.<sup>16,22,31,32</sup> We believe these uncertainties to be quite conservative.

The uncertainty in the noble gas density depends on the accuracy of the pressure gauge, which was 0.1 Torr for the early data recorded at Lehigh and 0.01 Torr for the more recent data. The gauge accuracy was 0.5 Torr at Lyon, where typically higher noble gas densities were used. The uncertainty in the

noble gas density is also affected by the uncertainty in the potassium density since alkali displaces some of the noble gases in the hot zone of the heat pipe oven. We refer the reader to Refs. 16, 22, 31, and 32 for details of the determination of the uncertainties in the densities.

We incorporated the uncertainties in the potassium and argon densities into the dependent variable of the fitted empirical models for the fluorescence and polarization spectroscopy intensity ratios [Eqs. (9), (23), and (32)] using

$$\Delta R_{F,P} = \left| \frac{\partial R_{F,P}}{\partial n_{NG}} \right| \Delta n_{NG} + \left| \frac{\partial R_{F,P}}{\partial n_{alk}} \right| \Delta n_{alk} + \frac{\Delta I}{I^{dir}} (1 + R_{F,P}), \quad (33)$$

where  $\Delta n_{NG}$  and  $\Delta n_{alk}$  are the uncertainties in the noble gas density and the alkali atom density, respectively. The factor  $\Delta I$  is the uncertainty in the measured collisional and direct line intensities, which is determined from the recorded background noise levels.  $I^{dir}$  is the intensity of the direct line measured in direct fluorescence (Lyon), in probe laser induced fluorescence (Lehigh fluorescence measurements), or in transmission through the crossed polarizer (Lehigh polarization measurements). The partial derivatives appearing in Eq. (33) are given by

$$\left| \frac{\partial R_F}{\partial n_{NG,alk}} \right| = \left| \frac{\frac{k_{NG,alk}^{\Delta J}}{\Gamma}}{\frac{k_{NG}^{\Delta J}}{\Gamma} n_{NG} + \frac{k_{alk}^{\Delta J}}{\Gamma} n_{alk}} - \frac{\frac{k_{NG,alk}^Q}{\Gamma}}{1 + \frac{k_{NG}^Q}{\Gamma} n_{NG} + \frac{k_{alk}^Q}{\Gamma} n_{alk}} \right| R_F, \quad (34)$$

$$\left| \frac{\partial R_P}{\partial n_{NG,alk}} \right| = \left| \frac{\frac{k_{NG,alk}^{\Delta J}}{\Gamma} (1 - f_{NG,alk}^{\Delta J})}{\frac{k_{NG}^{\Delta J}}{\Gamma} (1 - f_{NG}^{\Delta J}) n_{NG} + \frac{k_{alk}^{\Delta J}}{\Gamma} (1 - f_{alk}^{\Delta J}) n_{alk}} - \frac{\frac{g_{NG,alk}}{\Gamma}}{1 + \frac{g_{NG}}{\Gamma} n_{NG} + \frac{g_{alk}}{\Gamma} n_{alk}} \right| R_P. \quad (35)$$

Finally, in the individual fits carried out for the Lyon data corresponding to large values of  $\Delta J$  ( $|\Delta J| \geq 5$ ), the quenching rate coefficients were fixed at values determined from global fits to the  $|\Delta J| \leq 4$  data. Therefore, additional terms must be added to Eq. (33),<sup>22</sup>

$$\begin{aligned} & \left| \frac{\partial R_F^{Lyon}}{\partial \left( \frac{k_{NG}^Q}{\Gamma} \right)} \right| \Delta \left( \frac{k_{NG}^Q}{\Gamma} \right) + \left| \frac{\partial R_F^{Lyon}}{\partial \left( \frac{k_{alk}^Q}{\Gamma} \right)} \right| \Delta \left( \frac{k_{alk}^Q}{\Gamma} \right) \\ &= \left| \frac{1}{1 + \frac{k_{NG}^Q}{\Gamma} n_{NG} + \frac{k_{alk}^Q}{\Gamma} n_{alk}} \right| R_F^{Lyon} \\ & \quad \times \left[ n_{NG} \Delta \left( \frac{k_{NG}^Q}{\Gamma} \right) + n_{alk} \Delta \left( \frac{k_{alk}^Q}{\Gamma} \right) \right]. \quad (36) \end{aligned}$$

These expressions were used to assign uncertainties to each individual  $R_F$  and  $R_P$  value included in the fits.

## IV. DATA ANALYSIS AND FITTING

### A. Rotationally inelastic collisions of NaK $2(A)^1\Sigma^+(v = 16, J = 30)$ molecules

New data were collected using the Lehigh OODR fluorescence and polarization spectroscopy setup for helium and alkali atom  $J$ -changing collisions following excitation of the NaK  $2(A)^1\Sigma^+(v = 16, J = 30)$  level. These data were combined with the extensive set of data previously collected by Wolfe *et al.*<sup>16,32</sup> for collisions of NaK  $2(A)^1\Sigma^+(v = 16, J = 30)$  molecules with argon and alkali atoms and with new data collected in Lyon using the Fourier transform fluorescence setup. In these combined experiments, the noble gas pressure and oven temperature were varied to provide data covering as wide a range as possible in perturber densities,  $n_{NG}$  and  $n_{alk}$ . Unfortunately, there are upper limits on the viable ranges of both the temperature and pressure which can be used successfully since we want to keep the noble gas and alkali densities sufficiently low such that the single collision model remains approximately valid ( $k_p^{\Delta J} n_p \ll \Gamma_C + \sum_p k_p^{Q-C} n_p$ ). Conversely, if the temperature and/or pressure is too low, the collisional line signals cannot be recorded with adequate signal-to-noise ratio. As we discuss in Subsection 3 of the Appendix, it is not always possible to work strictly in the single-collision regime, and multiple collision effect corrections are sometimes needed.<sup>22</sup>

The Lehigh OODR experiment employed a two-step process to excite molecules from the ground state [NaK  $1(X)^1\Sigma^+(v = 0, J = 29)$ ] to the intermediate state [NaK  $2(A)^1\Sigma^+(v = 16, J = 30)$ ] with the pump laser, followed by probe laser excitation from the directly populated level or from a collisionally populated level to the upper state [NaK  $3^1\Pi(v = 6 \text{ or } 7, J = 30 \pm 1 \text{ or } J = 30 + \Delta J \pm 1)$ ]. If narrowband lasers are used, the OODR technique is Doppler-free so that intrinsic line shapes can be observed. In observing the direct and collisional lines at Lehigh, we have noticed that the collisional lines are broader than the direct lines (see Refs. 16, 31, and 32). Although both collisional and direct lines are broadened similarly by pressure broadening, the collisional lines experience additional broadening due to the collisions they have suffered, which can change the velocity of the molecule and hence re-introduce some Doppler broadening. Therefore, in taking ratios of collisional to direct line intensities, peak areas were used. For the Lyon fluorescence experiments, the line widths are limited by the resolution of the Fourier-transform spectrometer, and therefore intensity ratios were determined from peak heights.

The Lehigh OODR fluorescence data were fit using Eq. (23) while the limited amount of Lyon Fourier transform fluorescence data for NaK  $2(A)^1\Sigma^+(v = 16, J = 30)$  were fit with the very similar equation (11). The Lehigh polarization data were fit using Eq. (32). In all cases, the weighted  $R_F$  and  $R_P$  values were fit using the nonlinear multiple regression tool of Origin version 7.5. We assume that the rate coefficients  $k_p^{\Delta J}$  are different for different  $\Delta J$  values but that the total quenching rate coefficients  $k_p^{Q-C}$  can be taken to be the same for neighboring levels  $2(A)^1\Sigma^+(v = 16, J = 30 + \Delta J)$  where  $|\Delta J| \leq 4$ . This approximation is validated by the theoretical

calculations presented below. As in the case of Wolfe *et al.*,<sup>16</sup> we found that, for the polarization data fits, the parameter  $g'_p$  is highly correlated to the  $f_p^{\Delta J}$  and  $k_p^{Q-C}$  values and often fails to converge to a finite value if left to vary in the fitting process. Therefore, following Wolfe *et al.*, we fixed the values of  $g'_p$  to the expression

$$g'_p = \frac{1}{2} \left( f_p^{\Delta J=-1} k_p^{\Delta J=-1} + f_p^{\Delta J=+1} k_p^{\Delta J=+1} \right) \quad (37)$$

corresponding to the assumption that the rate coefficients for collisions that destroy orientation but do not change  $J$  should be approximately equal to the average of the rate coefficients for collisions that change  $J$  by  $\pm 1$  and simultaneously destroy orientation. Although this assumption seems reasonable, there is no *a priori* reason to believe it is true. Nevertheless, we find that setting the  $g'_p$  values to zero in the fits for any species  $p$  does not change the corresponding values of  $f_p^{\Delta J}$  and  $k_p^{Q-C}$  by more than a few percent due to the fact that  $g'_p$  calculated from Eq. (37) is more than an order of magnitude smaller than the corresponding  $k_p^{Q-C}$  value. An ongoing experiment with  $\text{Li}_2 A^1\Sigma_u^+$  molecules and argon perturbers also suggests that the rate coefficient for collisions that change  $M_J$  but not  $J$  is smaller than the rate coefficient for collisions in which  $J$  changes.<sup>33</sup>

Several different methods of fitting the data were tried. The principal method, which we call the “global fit” method, simultaneously fits all fluorescence and polarization data for both argon and helium perturbers. The equations for the fluorescence [Eqs. (11) and (23)] and polarization [Eq. (32)] intensity ratios share the global parameters  $k_{\text{He}}^{Q-C}$ ,  $k_{\text{Ar}}^{Q-C}$ , and  $k_{\text{alk}}^{Q-C}$ , while data recorded with helium and argon as the main buffer gas still share the alkali parameters  $k_{\text{alk}}^{\Delta J}$ ,  $f_{\text{alk}}^{\Delta J}$ , and  $k_{\text{alk}}^Q$ .

We note that the fitting process must be iterated since the uncertainties in the individual  $R_F$  and  $R_P$  values depend on the fitted parameters [see Eqs. (33)–(35)], which in turn depend on those same uncertainties. In the global fit method, and in each of the other fits described below, initial values of the fitting parameters were chosen and initial values of the uncertainties in the  $R_F$  and  $R_P$  values were calculated using Eqs. (33)–(35). A fitting run was carried out for some number of iterations (usually to convergence). Then the uncertainties in the  $R_F$  and  $R_P$  values were updated and the data refit. This process was continued until the values of the fitting parameters (and hence also the values of the error bars in the  $R_{F,P}$  values) no longer changed from one round of fitting to the next. The radiative rate  $\Gamma = 4.4 \times 10^7 \text{ s}^{-1}$  was determined from the program LEVEL,<sup>34</sup> using the ground state  $1(X)^1\Sigma^+$  potential of Refs. 35 and 36, the  $2(A)^1\Sigma^+$  state potential of Ref. 28, and the transition dipole moment of Ref. 37.

In the second fitting method, called the “separate buffer gas fit,” we first fit the more extensive argon fluorescence and polarization data, together with heat pipe mode data where the noble gas is excluded from the interaction region, to yield the parameters  $k_{\text{Ar}}^{\Delta J}$ ,  $k_{\text{Ar}}^{Q-C}$ ,  $f_{\text{Ar}}^{\Delta J}$ ,  $k_{\text{alk}}^{\Delta J}$ ,  $k_{\text{alk}}^{Q-C}$ , and  $f_{\text{alk}}^{\Delta J}$ . The alkali parameters were then fixed at the values obtained in this fit of the argon data and used in a subsequent fit of the helium fluorescence and polarization data. In the third fitting method, called the “fluorescence and polarization fit,” we first fit all argon and

helium fluorescence data together to obtain the parameters  $k_{\text{Ar}}^{\Delta J}$ ,  $k_{\text{Ar}}^{Q-C}$ ,  $k_{\text{He}}^{\Delta J}$ ,  $k_{\text{He}}^{Q-C}$ ,  $k_{\text{alk}}^{\Delta J}$ , and  $k_{\text{alk}}^{Q-C}$ . These values were then fixed in a subsequent fit of the polarization data to obtain the  $f_p^{\Delta J}$  values. Finally, in the fourth method, called the “fully separated fit,” we first fit the argon fluorescence data to yield the  $k_{\text{Ar}}^{\Delta J}$ ,  $k_{\text{Ar}}^{Q-C}$ ,  $k_{\text{alk}}^{\Delta J}$ , and  $k_{\text{alk}}^{Q-C}$  values. Then we fixed all of these values in a subsequent fit of the argon polarization data to yield  $f_{\text{Ar}}^{\Delta J}$  and  $f_{\text{alk}}^{\Delta J}$ . The parameters  $k_{\text{alk}}^{\Delta J}$  and  $k_{\text{alk}}^{Q-C}$  were also fixed in a fit of the helium fluorescence data to obtain  $k_{\text{He}}^{\Delta J}$  and  $k_{\text{He}}^{Q-C}$ . Then parameters  $k_{\text{He}}^{\Delta J}$ ,  $k_{\text{He}}^{Q-C}$ ,  $k_{\text{alk}}^{\Delta J}$ ,  $k_{\text{alk}}^{Q-C}$ , and  $f_{\text{alk}}^{\Delta J}$  were fixed at the values already determined, in a fit of the helium polarization data to yield  $f_{\text{He}}^{\Delta J}$ . Values of the various fitted parameters obtained from the different methods are in good agreement with each other and are given in the [supplementary material](#) (Tables 1–8 and Figs. 1–8) along with plots showing comparisons of the various measured helium fluorescence and polarization intensity ratios with the predictions of Eqs. (11), (23), and (32) using the parameters obtained in the global fit (Figs. 9–24 of the [supplementary material](#)). Similar comparisons for the argon data appeared in the work of Wolfe *et al.*<sup>16</sup> (see Figs. 6 and 7 and the supplementary material of that work).

Rate coefficients determined from these fits are presented in Sec. V. We consider values obtained from the global fit to be the most reliable since all parameters are fit simultaneously in this method.

## B. Inelastic collisions of $\text{NaK } 2(A)^1\Sigma^+(v=0, J=14)$ , $(v=0, J=30)$ , $(v=1, J=26)$ , and $(v=2, J=44)$ molecules with argon and helium atoms

All of the data involving collisional transitions following laser excitation of the NaK intermediate levels  $2(A)^1\Sigma^+(v=0, J=14)$ ,  $(v=0, J=30)$ ,  $(v=1, J=26)$ , and  $(v=2, J=44)$  from ground state levels  $1(X)^1\Sigma^+(v=6, J=15)$ ,  $(v=6, J=31)$ ,  $(v=4, J=25)$ , and  $(v=4, J=43)$ , respectively, were collected using the FTS system in Lyon. The operating wavelength range of the laser system in Lyon is better suited to accessing these low-lying ro-vibrational levels of the NaK  $2(A)^1\Sigma^+$  state. However, these data are limited to population transfer information only.

Both argon and helium were used as the NaK molecule collision partner, with noble gas densities ranging between  $3 \times 10^{16}$  and  $3 \times 10^{17} \text{ cm}^{-3}$ . In these experiments, the alkali (potassium) density was kept much lower than the noble gas density, typically in the range  $1 \times 10^{14} - 3 \times 10^{15} \text{ cm}^{-3}$ .

From the spectra, we determined relative collisional to direct line fluorescence intensity ratios,  $\frac{I_{C \rightarrow \ell_C}}{I_{D \rightarrow \ell_D}}$ , for the observed collisional lines  $C = D + \Delta J$ . The range of  $\Delta J$  was truncated to include only those values where the signal-to-noise ratio was considered sufficiently good to carry out a meaningful fit. We assigned an uncertainty calculated using Eqs. (33)–(36) to each measured intensity ratio and then fit the data using Eq. (9). In principle it should be possible to fit the data corresponding to each individual collisional line and determine the parameters  $\frac{k_{\text{NG}}^{\Delta J}}{\Gamma_C}$ ,  $\frac{k_{\text{alk}}^{\Delta J}}{\Gamma_C}$ ,  $\frac{k_{\text{NG}}^{Q-C}}{\Gamma_C}$ , and  $\frac{k_{\text{alk}}^{Q-C}}{\Gamma_C}$  for each  $\Delta J$  value separately. In practice, the  $J$ -changing collision rates and the quenching rates are somewhat correlated and the data set is not sufficiently robust to obtain meaningful values from this type of fit.

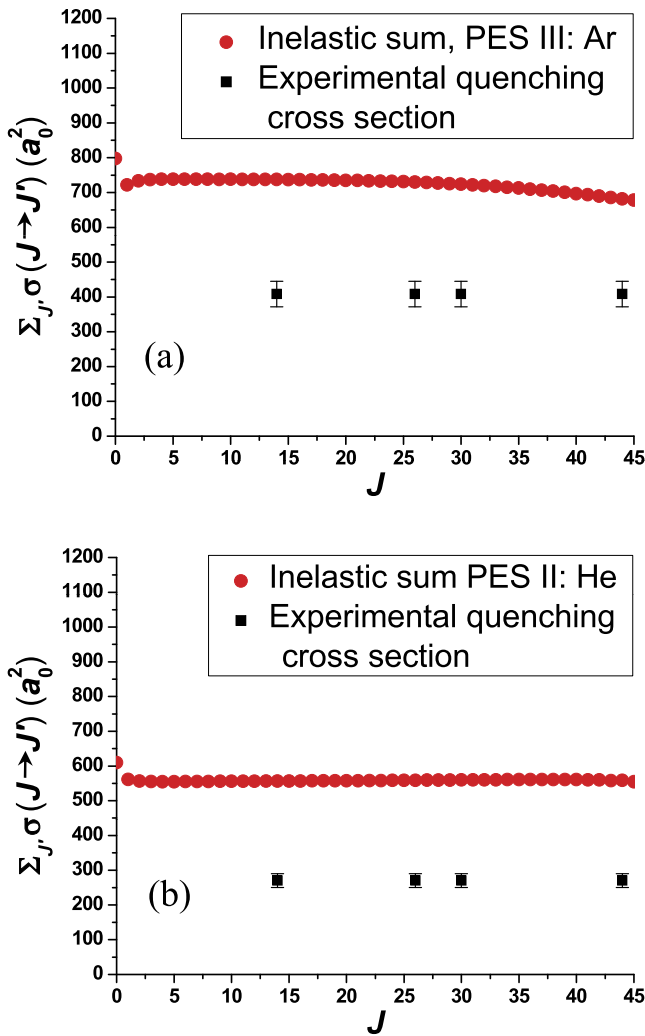


FIG. 6. Sum of rotationally inelastic cross sections  $\sum_{J' \neq J} \sigma(J \rightarrow J')$ , as a function of initial  $J$ , for collisions of NaK  $2(A)^1\Sigma^+$  ( $v = 0, J$ ) molecules, with (a) argon, and (b) helium perturbers. These results demonstrate that the quenching rates are mostly independent of the rotational level. Initial  $J$  was limited to 45 in both cases to ensure that the sums had converged. The codes PES III: Ar and PES II: He in the legends refer to potential energy surfaces calculated in Ref. 21.

However, our calculations of total inelastic (rotation-changing) collision cross sections,  $\sum_{\Delta J} \sigma^{J \rightarrow J+\Delta J}$ , which serve as reasonable proxies for the quenching cross sections, are approximately independent of the initial state  $J$  (see Fig. 6).<sup>21</sup> In addition, the calculations show that the quenching cross sections are also approximately independent of  $v$  (see Fig. 47 of the [supplementary material](#)). Therefore we decided to carry out a global fit of all of the Lyon data for  $|\Delta J| \leq 4$  that were obtained with various argon and helium densities and all four of the directly excited NaK  $2(A)^1\Sigma^+$  levels studied [ $(v = 0, J = 14)$ ,  $(v = 0, J = 30)$ ,  $(v = 1, J = 26)$ , and  $(v = 2, J = 44)$ ]. In this fit, the quenching coefficients  $k_{\text{Ar}}^{Q-C}$ ,  $k_{\text{He}}^{Q-C}$ , and  $k_{\text{K}}^{Q-C}$  were taken to be global parameters (independent of the directly excited level  $D$  and of the collisional level  $C$ ), but the individual population transfer rate coefficients  $k_{\text{Ar}}^{\Delta J}$ ,  $k_{\text{He}}^{\Delta J}$ , and  $k_{\text{K}}^{\Delta J}$  were considered to be independent for each type of perturber, each value of  $\Delta J$ , and each pump transition. This defined a 99-parameter fit (96 rate coefficients for the transitions from

$J$  to  $J + \Delta J$  induced by each of the three perturbers, for four initial values of  $J$  and eight values of  $\Delta J$ , plus three global quenching rate coefficients). Results of this fit are reported in Sec. V.

To test whether this fit is robust, we also tried various other fits in which one or more of the quenching rate coefficients were set to specific values. In one fit, we fixed all quenching rate coefficients at the values obtained in the  $v = 16, J = 30$  global fit ( $k_{\text{Ar}}^Q/\Gamma_C = 2.81 \times 10^{-17} \text{ cm}^3$ ,  $k_{\text{He}}^Q/\Gamma_C = 4.15 \times 10^{-17} \text{ cm}^3$ , and  $k_{\text{K}}^Q/\Gamma_C = 2.69 \times 10^{-16} \text{ cm}^3$ ). Since the potassium densities have large uncertainties, we also tried fixing the potassium quenching rate coefficient  $k_{\text{K}}^Q/\Gamma_C$  to various fixed values between 0 and  $10^{-15} \text{ cm}^3$  while allowing the noble gas quenching coefficients to vary. However, we found that the fitted values of the noble gas population transfer rate coefficients were very insensitive to the value of the potassium quenching rate coefficient. The fact that the best values of the noble gas and alkali quenching rate coefficients obtained from the global fit of the data for the four low  $v$  pump transitions obtained in Lyon [ $k_{\text{Ar}}^Q/\Gamma_C = (1.76 \pm 0.16) \times 10^{-17} \text{ cm}^3$ ,  $k_{\text{He}}^Q/\Gamma_C = (2.96 \pm 0.22) \times 10^{-17} \text{ cm}^3$ , and  $k_{\text{K}}^Q/\Gamma_C = (4.30 \pm 1.05) \times 10^{-16} \text{ cm}^3$ ] are not very different from the values obtained from the fit of the  $v = 16$  data also supports the idea that the quenching rate coefficients can be taken to be approximately independent of  $v$  and  $J$ .

Once the global fit of the Lyon  $|\Delta J| \leq 4$  data was completed, we carried out individual fits of the data obtained with larger values of  $|\Delta J|$ , with the quenching rate coefficients fixed at the values obtained in the global fit. For each  $\Delta J$ , and each pump transition, the values of  $k_{\text{Ar}}^{\Delta J}/\Gamma_C$ ,  $k_{\text{He}}^{\Delta J}/\Gamma_C$ , and  $k_{\text{K}}^{\Delta J}/\Gamma_C$  were determined in a 3-parameter fit. In this case, since the quenching rate coefficients were fixed, the uncertainties in each data point had to be supplemented by the additional terms in Eq. (36). Since the quenching coefficients are taken to be the same for all pump transitions and all  $\Delta J$  values, we believe the fitting procedure described here provides the most accurate values for *relative* population transfer rate coefficients for different values of  $\Delta J$ . However, there are fairly large uncertainties in the absolute rate coefficients due to the inability to accurately account for multiple collision effects, as discussed in Subsection 3 of the Appendix.

The fitting parameters  $k_p^{\Delta J}/\Gamma_C$  were converted to rate coefficients  $k_p^{\Delta J}$  using the radiative rate  $\Gamma = 4.7 \times 10^7 \text{ s}^{-1}$ , which was determined from the program LEVEL,<sup>34</sup> using the ground state  $1(X)^1\Sigma^+$  potential of Refs. 35 and 36, the  $2(A)^1\Sigma^+$  state potential of Ref. 28, and the transition dipole moment of Ref. 37. Values of  $k_{\text{Ar}}^{\Delta J}$  and  $k_{\text{He}}^{\Delta J}$  obtained in the Lyon experiment for each of the four pump transitions with  $v = 0, 1$ , and 2 are presented in Sec. V A and the [supplementary material](#).

## V. RESULTS AND COMPARISON WITH THEORY

### A. Results for NaK

#### 1. Population transfer and quenching

Experimental rate coefficients  $k_p^{\Delta J}$  for  $J$ -changing collisions of NaK  $2(A)^1\Sigma^+$  with various perturbers  $p$  and for several

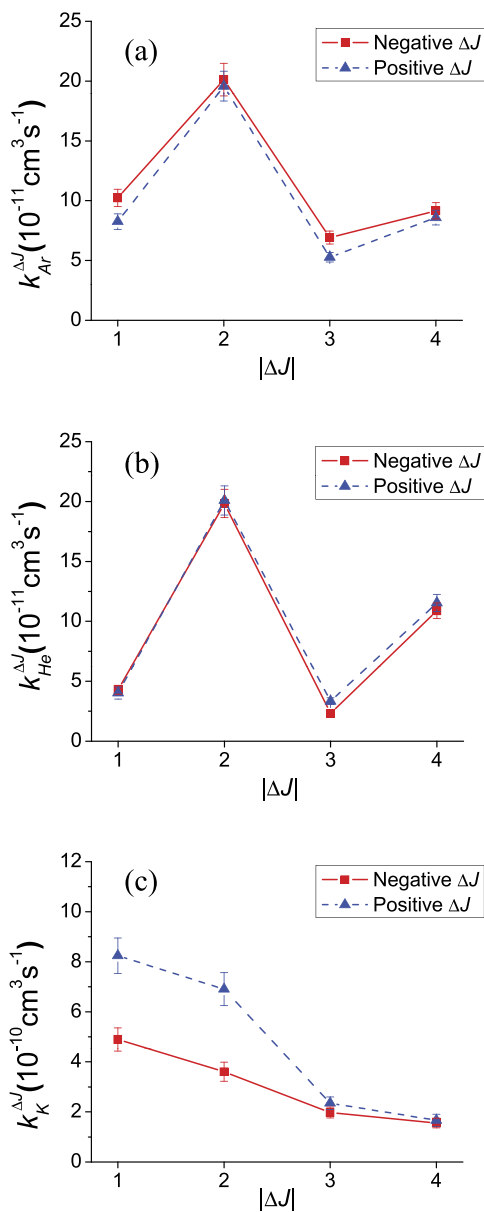


FIG. 7. Experimental rate coefficients,  $k_{Ar}^{\Delta J}$ ,  $k_{He}^{\Delta J}$ , and  $k_K^{\Delta J}$ , for collisions of NaK  $2(A)^1\Sigma^+(v = 16, J = 30)$  molecules with (a) argon, (b) helium, and (c) potassium atoms as functions of  $\Delta J$ .

different initial levels ( $v, J$ ) are shown in Figs. 7–10 here and Figs. 25 and 27–30 of the [supplementary material](#). Numerical values are tabulated in Table I and in Tables 1, 3, 5, 7, and 9–12 of the [supplementary material](#). Table I and Tables 1, 3, 5, and 7 of the [supplementary material](#) also give the measured quenching rate coefficients  $k_{Ar}^Q$ ,  $k_{He}^Q$ , and  $k_K^Q$ .

Values of the rate coefficients  $k_p^{\Delta J}$  for  $J$ -changing collisions of NaK  $2(A)^1\Sigma^+(v = 16, J = 30)$  molecules with argon, helium, and potassium perturbors are plotted in Fig. 7 and are listed in Table I. These rates are from the global fit of the Lehigh measurements described in Sec. IV A. Panels (a) and (b) for argon and helium show a clear propensity for  $\Delta J = \text{even}$  transitions. No  $\Delta J = \text{even}$  propensity is observed in panel (c) for potassium. The  $k_K^{\Delta J}$  decrease monotonically with increasing  $|\Delta J|$ , and the largest values are three

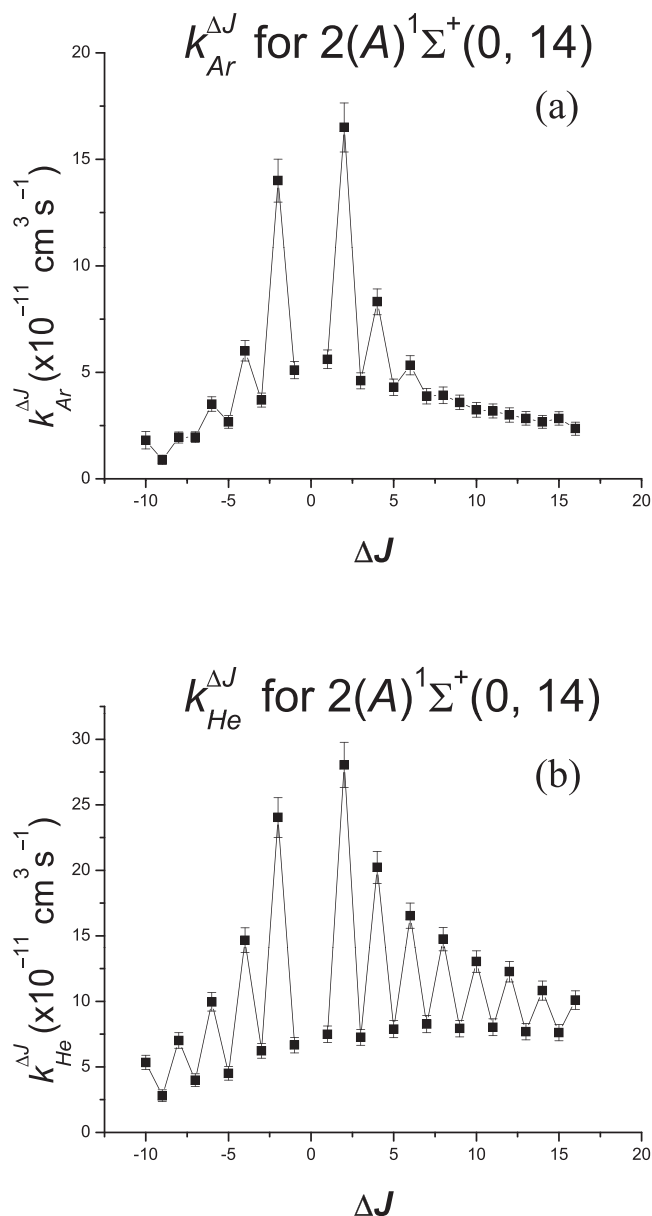
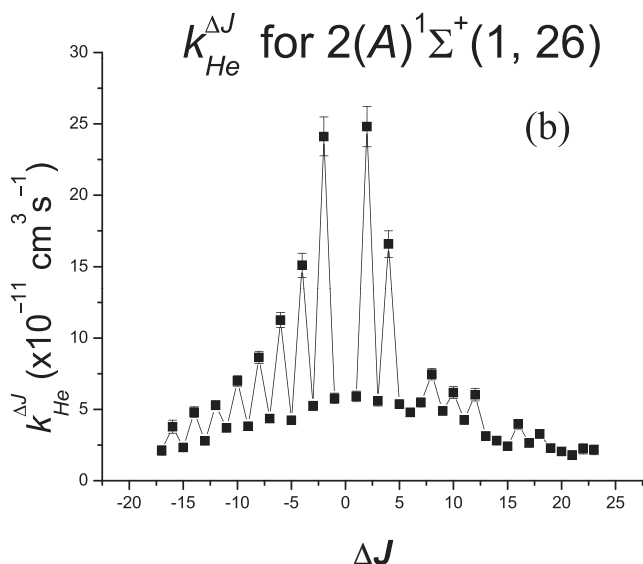
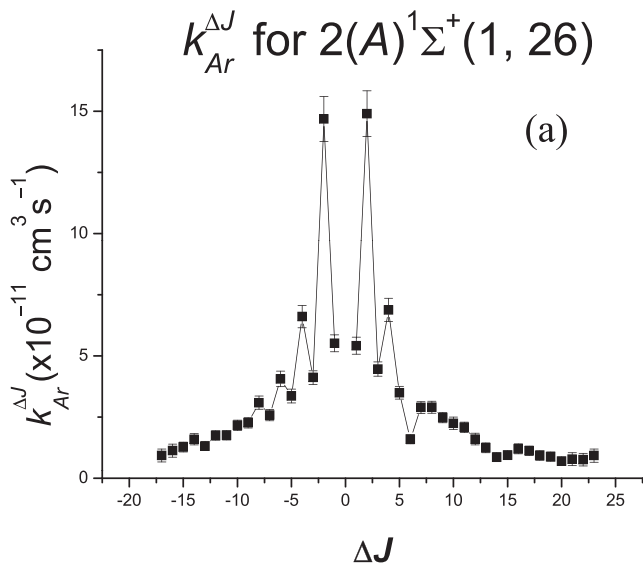


FIG. 8. Rate coefficients for rotationally inelastic collisions of NaK  $2(A)^1\Sigma^+(v = 0, J = 14)$  molecules with (a) argon and (b) helium atoms as functions of  $\Delta J$ .

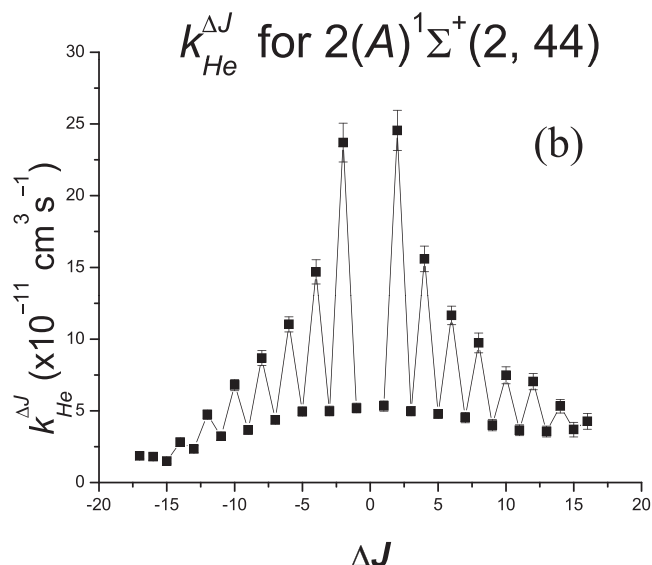
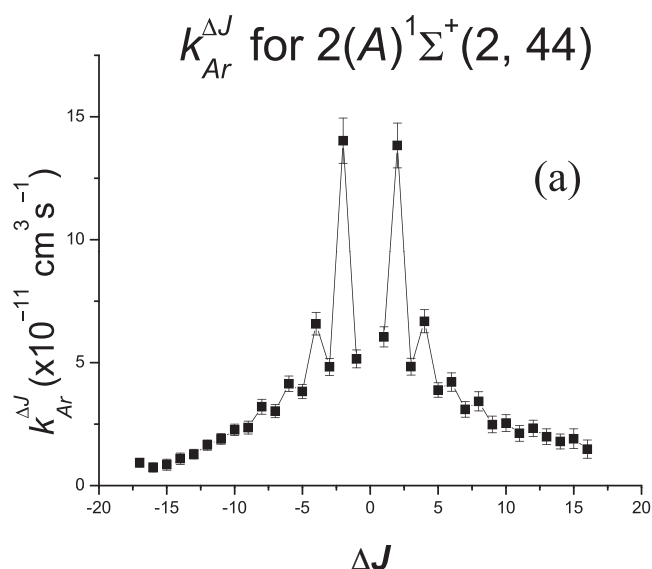
or four times larger than the maximum rates for helium or argon.

The values of  $k_{Ar}^{\Delta J}$  and  $k_{He}^{\Delta J}$  for the (0, 14), (1, 26), and (2, 44) pump transitions are shown in Figs. 8–10 (see also Tables 9, 11, and 12 of the [supplementary material](#)). These rate coefficients are from the fits of the Lyon measurements described in Sec. IV B. Additional results showing the best fit values for  $k_K^{\Delta J}$  for all pump transitions used in Lyon and for  $k_{Ar}^{\Delta J}$  and  $k_{He}^{\Delta J}$  for the (0, 30) pump transition are also provided in Figs. 27–30 and Tables 9–12 of the [supplementary material](#). The general dependence of the rate coefficients for argon and helium as a function of  $\Delta J$  is very similar for the different initial states although the magnitudes vary. The maximum rate coefficients for helium tend to be larger than those for argon and to have a more pronounced  $\Delta J = \text{even}$  propensity, especially for larger  $|\Delta J|$ . Close examination shows an anomaly in Fig. 9 for both argon and helium. The  $\Delta J = 6$  rate

FIG. 9. Same as in Fig. 8, but for ( $v = 1, J = 26$ ).

coefficients are strongly suppressed; there are no peaks at  $\Delta J = 6$  as there are in the corresponding transitions in Figs. 8 and 10. This effect arises from the spin-orbit coupling between  $2(A)^1\Sigma^+$  and the nearby  $1(b)^3\Pi$  state and is part real and part artifact. A more detailed explanation is given in Sec. V A 4.

Our recent calculations<sup>20,21</sup> allow a close comparison with these experimental results. We obtained results for collisions of NaK  $2(A)^1\Sigma^+(v = 0)$  molecules with argon for  $J \leq 50$  and with helium for  $J \leq 60$ . We also estimated the dependence of the cross sections on the initial value of  $v$  by repeating the coupled channel calculations using a potential averaged over the  $v$ th vibrational wave function. This method was used by Malenda *et al.*<sup>18</sup> and should be justified when vibrationally inelastic cross sections are small, as preliminary results<sup>22</sup> for the present case suggest. A rigorous comparison with the measured rate coefficients would involve a convolution over the experimental energy distribution at  $T \approx 600$  K,

FIG. 10. Same as in Fig. 8, but for ( $v = 2, J = 44$ ).

but extending our calculations to the high end of this distribution is not feasible. Fortunately, the cross sections do not vary greatly over the range we have studied, so we can approximate

$$k_P^{\Delta J} = \langle v\sigma_P^{\Delta J}(v) \rangle \approx \bar{v}\sigma_P^{\Delta J}(\bar{v}), \quad (38)$$

where  $v$  is the collision velocity, the angular brackets indicate a thermal average and  $\bar{v}$  is the mean relative velocity.

Figures 11 and 12 compare experimental rate coefficients to theoretical estimates based on Eq. (38). The calculated rate coefficients are in very good agreement with the experimental data. The calculations reproduce the observed propensity for  $\Delta J = \text{even}$  transitions, and in most cases, the absolute magnitudes of the calculations are within experimental error bars. Experiment and theory agree that collisions with helium show a stronger propensity for  $\Delta J = \text{even}$  transitions than do collisions with argon.

The calculations for Ar + NaK shown in Figs. 11(a) and 12(a) also exhibit a slight propensity for  $\Delta J = \text{odd}$  transitions for  $|\Delta J| \geq 7$ . Experimental uncertainties are sufficiently

TABLE I. Global fit rate coefficients ( $k_p^{\Delta J}$ ) in units of the radiative rate  $\Gamma$  and in units of  $\text{cm}^3 \text{s}^{-1}$  [the latter obtained by multiplying the fitted parameters ( $k_p^{\Delta J}/\Gamma$ ) by  $\Gamma = 4.4 \times 10^7 \text{ s}^{-1}$ ] for rotationally inelastic population transfer collisions of NaK  $2(A)^1\Sigma^+(v = 16, J = 30)$  with argon, helium, and potassium atoms ( $p = \text{Ar, He, and K}$ ). Quenching rate coefficients are also given.

$\Delta J$	$k_{\text{Ar}}^{\Delta J}/\Gamma$	$k_{\text{He}}^{\Delta J}/\Gamma$	$k_{\text{K}}^{\Delta J}/\Gamma$	$k_{\text{Ar}}^{\Delta J}$	$k_{\text{He}}^{\Delta J}$	$k_{\text{K}}^{\Delta J}$
	( $10^{-18} \text{ cm}^3$ )	( $10^{-18} \text{ cm}^3$ )	( $10^{-17} \text{ cm}^3$ )	( $10^{-11} \text{ cm}^3 \text{ s}^{-1}$ )	( $10^{-11} \text{ cm}^3 \text{ s}^{-1}$ )	( $10^{-10} \text{ cm}^3 \text{ s}^{-1}$ )
-4	$2.08 \pm 0.15$	$2.47 \pm 0.15$	$0.35 \pm 0.04$	$9.16 \pm 0.68$	$10.89 \pm 0.66$	$1.56 \pm 0.20$
-3	$1.57 \pm 0.12$	$0.53 \pm 0.05$	$0.45 \pm 0.05$	$6.93 \pm 0.54$	$2.32 \pm 0.22$	$1.97 \pm 0.22$
-2	$4.57 \pm 0.31$	$4.51 \pm 0.27$	$0.82 \pm 0.09$	$20.13 \pm 1.36$	$19.84 \pm 1.18$	$3.61 \pm 0.38$
-1	$2.33 \pm 0.16$	$0.98 \pm 0.08$	$1.11 \pm 0.11$	$10.23 \pm 0.72$	$4.29 \pm 0.36$	$4.90 \pm 0.46$
0						
1	$1.88 \pm 0.15$	$0.91 \pm 0.11$	$1.87 \pm 0.16$	$8.25 \pm 0.65$	$4.02 \pm 0.51$	$8.24 \pm 0.71$
2	$4.45 \pm 0.28$	$4.57 \pm 0.28$	$1.57 \pm 0.15$	$19.57 \pm 1.24$	$20.09 \pm 1.22$	$6.91 \pm 0.66$
3	$1.20 \pm 0.09$	$0.76 \pm 0.06$	$0.53 \pm 0.06$	$5.27 \pm 0.40$	$3.35 \pm 0.28$	$2.35 \pm 0.25$
4	$1.95 \pm 0.14$	$2.62 \pm 0.16$	$0.38 \pm 0.05$	$8.59 \pm 0.61$	$11.54 \pm 0.71$	$1.66 \pm 0.24$
	$k_{\text{Ar}}^Q/\Gamma$	$k_{\text{He}}^Q/\Gamma$	$k_{\text{K}}^Q/\Gamma$	$k_{\text{Ar}}^Q$	$k_{\text{He}}^Q$	$k_{\text{K}}^Q$
	( $10^{-18} \text{ cm}^3$ )	( $10^{-18} \text{ cm}^3$ )	( $10^{-17} \text{ cm}^3$ )	( $10^{-11} \text{ cm}^3 \text{ s}^{-1}$ )	( $10^{-11} \text{ cm}^3 \text{ s}^{-1}$ )	( $10^{-10} \text{ cm}^3 \text{ s}^{-1}$ )
	$28.1 \pm 2.5$	$41.5 \pm 3.4$	$26.9 \pm 2.8$	$123.7 \pm 11.0$	$182.6 \pm 15.0$	$118.5 \pm 12.5$

large that the current data cannot provide a definitive test of this prediction. The semiclassical analysis by McCurdy and Miller<sup>38</sup> showed that the  $\Delta J = \text{even}$  propensity is sensitive to the degree to which the atom-diatom PES deviates from symmetry under the exchange of the two nuclei of the molecule; by using a simplified PES with adjustable parameters, McCurdy and Miller showed that in certain cases a propensity for  $\Delta J = \text{odd}$  transitions appeared. Our calculations for Ar + NaK are consistent with this prediction even though our PES has a different form than that used by McCurdy and Miller. We have performed additional studies related to this point, which are discussed in Ref. 21 and which will be published at a later date.

Figures 11 and 12 also provide information about the dependence of  $k_{\text{Ar}}^{\Delta J}$  and  $k_{\text{He}}^{\Delta J}$  on the initial level ( $v, J$ ). The rate coefficients (both experimental and theoretical) for each perturber in the two figures are very similar, suggesting that the dependence is weak for the range of  $v$  and  $J$  investigated. In fact, the dependence of  $k_{\text{He}}^{\Delta J}$  on  $v$  and  $J$  in the calculations of Malenda *et al.* was negligible for  $v \leq 7$  and  $14 \leq J \leq 30$  (see Fig. 8 of Ref. 18).

Figure 13 provides additional information about the dependence of the rate coefficients on the initial value of  $J$ . Calculated cross sections,  $\sigma(J \rightarrow J')$ , are shown as a function of initial  $J$  for fixed  $\Delta J$ , along with the corresponding experimental results (determined by dividing the experimental rate coefficients by the mean relative velocity,  $\bar{v}$ ). The experimental and calculated cross sections for fixed  $\Delta J$  depend very weakly on initial  $J$  in the observed range  $14 \leq J \leq 44$  although the  $J$ -dependence of the theoretical cross sections for lower  $J$  is much stronger. Most of the cross sections increase or decrease sharply as  $J$  drops below  $\sim 10$ . The experimental data pairs for  $J = 14$  and fixed  $|\Delta J|$  clearly exhibit greater splitting than the corresponding pairs for  $J \geq 26$ ; the calculations show the same pattern. Part of this behavior may be attributed to the principle of detailed balance, but the details of the PES may play a role.

Finally, we note that the calculations predict a qualitatively different behavior between transitions with odd and even  $\Delta J$ , for He + NaK, as shown in panels (c) and (d) of Fig. 13.

## 2. Collisional transfer of orientation

The measured fractions of orientation destroyed,  $f_p^{\Delta J}$ , obtained from the global fit of the Lehigh data described in Sec. IV A, for perturbers  $p = \text{argon, helium, and potassium atoms}$  in collisions with NaK  $2(A)^1\Sigma^+(v = 16, J = 30)$  molecules are presented in Fig. 14. These values are also listed in Table II, along with the fixed values of  $g'_p$  used in the fit. Experimental values obtained using the other fit methods are presented in Tables 2, 4, 6, and 8 of the [supplementary material](#). Figures 15(a) and 15(b) show comparisons of experimental and theoretical values of  $f_p^{\Delta J}$  for argon and helium, respectively.

Figure 14 clearly shows that the effectiveness with which a perturber destroys the orientation of NaK  $2(A)^1\Sigma^+(v = 16, J = 30)$  molecules varies greatly with the perturber. Panel (a) shows that collisions with argon cause a prepared ensemble of target molecules to lose about 1/3 to 2/3 of its initial orientation. The loss is greater for collisions with larger  $|\Delta J|$ . The corresponding loss for most values of  $\Delta J$  with helium is about 0%–25%. The value for  $\Delta J = -4$  is rather large at 61%; the origin of the sharp increase is unclear but is probably an experimental artifact since the signals are quite small in that case.

Panel (c) of Fig. 14 shows that collisions with potassium destroy 85%–100% of the initial orientation. This high value likely has to do with the fact that both potassium and NaK  $2(A)^1\Sigma^+$  are open shell systems and can interact very strongly. Although a rigorous calculation would be very involved, we have investigated<sup>21,39</sup> a model system with a very deep attractive well that roughly matches the interaction of the open shell systems Li and CN. The results show that the  $M_{J'}$

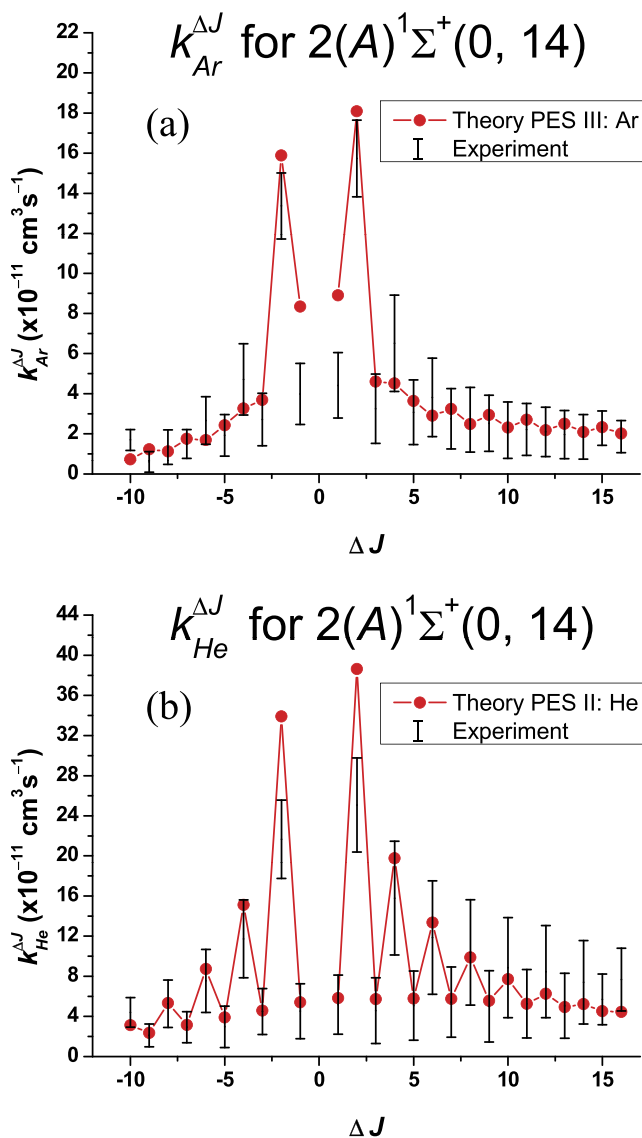


FIG. 11. Approximate theoretical (rigid rotor) rate coefficients for rotationally inelastic collisions of NaK  $2(A)^1\Sigma^+(v = 0, J = 14)$  molecules with (a) argon and (b) helium, as functions of  $\Delta J$ , in comparison with experimental rate coefficients. The codes PES III: Ar and PES II: He in the legends refer to potential energy surfaces calculated in Ref. 21. The upper limits of the experimental error bars are the upper limits of the “uncorrected” experimental rate coefficients shown in Fig. 8, while the lower limits of the experimental error bars are the rate coefficients corrected for multiple collision effects (see Subsection 3 of the Appendix, Fig. 16(a), and Fig. 31 of the [supplementary material](#)).

levels of final state  $J'$  of the molecule are almost completely randomized, and most of the orientation is destroyed. Such model calculations provide a plausible rationale for the large values of  $f_K^{\Delta J}$ .

A perfect comparison between theoretical and experimental values of  $f_{Ar}^{\Delta J}$  and  $f_{He}^{\Delta J}$  is still not possible. The data are for  $v = 16$ , while the calculations are for  $v = 0$ . We estimate, however, that the transfer of orientation does not depend strongly on the vibrational level  $v$ ; for  $\Delta J = \text{odd}$  transitions induced by helium and argon, our approximate calculations<sup>21</sup> show that at most 15% and 20% more orientation is destroyed, respectively, for  $v = 0$  than for  $v = 16$ , while for  $\Delta J = \text{even}$  transitions the results differ by much less. A second

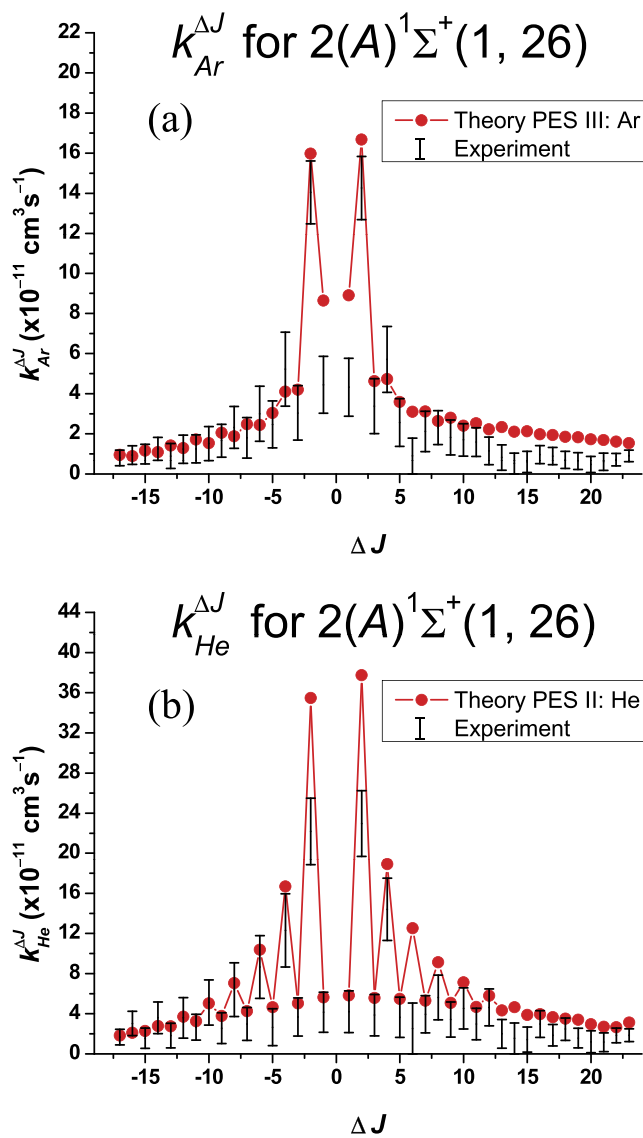
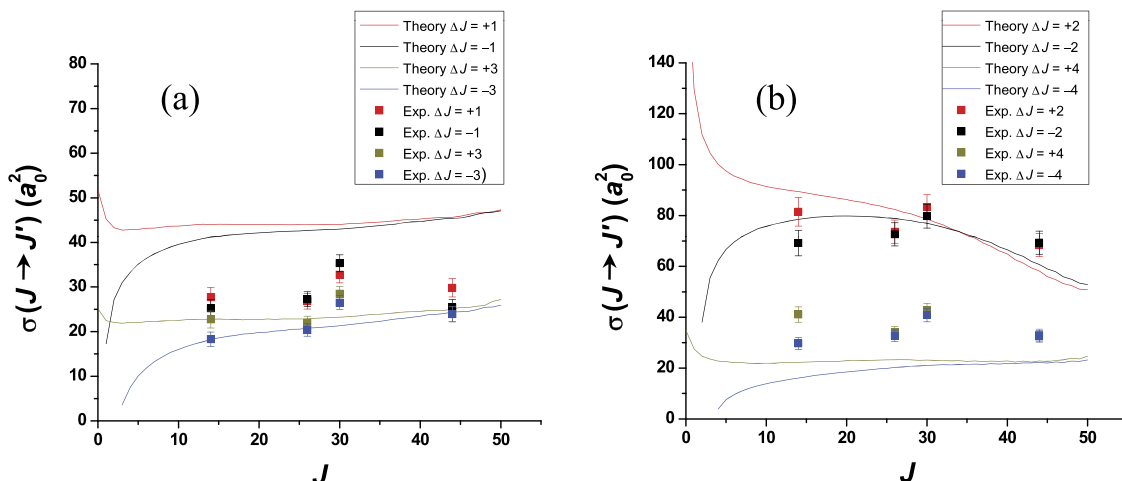


FIG. 12. Same as in Fig. 11 for  $(v = 1, J = 26)$ . The upper limits of the experimental error bars are the upper limits of the “uncorrected” experimental rate coefficients shown in Fig. 9, while the lower limits of the experimental error bars are the rate coefficients corrected for multiple collision effects (see Subsection 3 of the Appendix, and Fig. 33 of the [supplementary material](#)).

consideration affecting the comparison is that, just as with the rate coefficients, the experiments sample a Maxwellian distribution of collision energies, while the calculations are performed at the average collision energy. This uncertainty also affects the comparison.

Despite these uncertainties, we show in Fig. 15 the comparison of theoretical and experimental values of  $f_{Ar}^{\Delta J}$  and  $f_{He}^{\Delta J}$ . Panel (a) shows the result for argon collisions. The data show a greater loss of orientation than that predicted by the calculations. However, for both experiment and theory,  $f_{Ar}^{\Delta J}$  generally increases with increasing  $|\Delta J|$ , and there is a rough symmetry between positive  $\Delta J$  and negative  $\Delta J$ . This approximate symmetry arises naturally from the calculations at high  $J$ . As shown in the work of Malenda *et al.*,<sup>18</sup> the loss of orientation (for a given perturber) depends rigorously only on  $|\Delta J|$  and the average  $\bar{J} = (J + J')/2$ . In other words, the orientation loss in  $J \rightarrow J'$  and  $J' \rightarrow J$

## Ar + NaK, PES III: Ar



## He + NaK, PES II: He

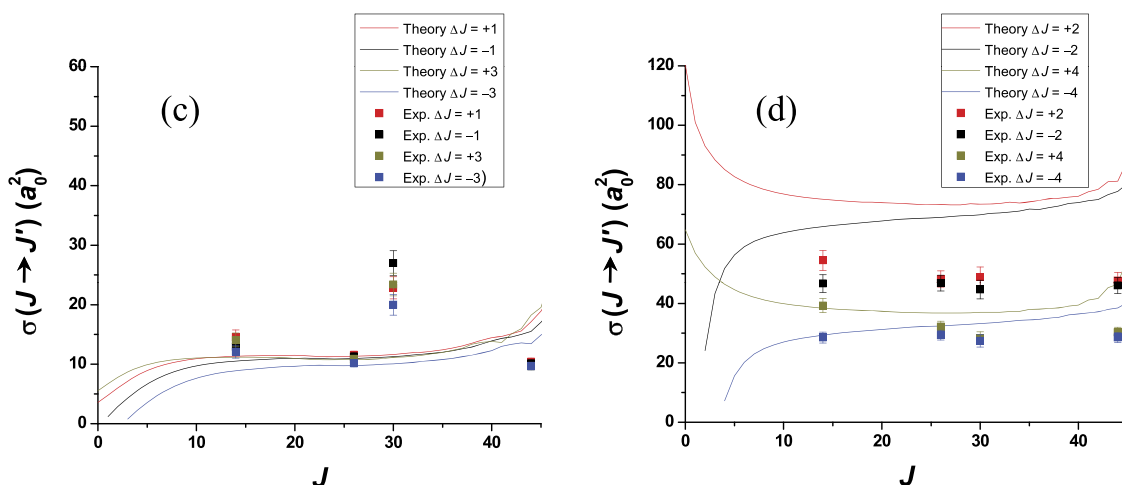


FIG. 13. Cross sections as a function of initial  $J$  for fixed  $\Delta J$  for (a) Ar + NaK,  $\Delta J = \text{odd}$ , (b) Ar + NaK,  $\Delta J = \text{even}$ , (c) He + NaK,  $\Delta J = \text{odd}$ , (d) He + NaK,  $\Delta J = \text{even}$ . The codes PES III: Ar and PES II: He in the titles refer to potential energy surfaces calculated in Ref. 21. The predicted difference between positive and negative  $\Delta J$  is more pronounced at low  $J$ , and is generally consistent with the experimental data. For He + NaK, the odd and even transitions show qualitatively different behavior.

transitions will be equal. For the present experimental situation,  $J$  rather than  $\bar{J}$  is fixed, so the symmetry is only approximate.

Figure 15(b) shows the results for helium collisions. For this case, the calculations are generally close to the measurements, within error bars for  $\Delta J = \text{odd}$  transitions and for  $\Delta J = +4$ , but outside of the error bars for  $\Delta J = \pm 2$  and  $\Delta J = -4$ . As in panel (a), the calculations exhibit an approximate symmetry between positive  $\Delta J$  and negative  $\Delta J$ . In this context, as in Fig. 14(b), the experimental result for  $\Delta J = -4$  is clearly anomalous.

A final comparison between panels (a) and (b) shows that for the same transition  $J \rightarrow J'$ , experiment and theory agree that collisions with argon destroy more of the orientation than collisions with helium do. Since argon is more massive and interacts more strongly with the molecule, this result is just what one might expect.

### 3. Multiple collision effects

Multiple collision effects cannot be neglected when the lifetime of the NaK  $2(A)^1\Sigma^+(v, J)$  level of interest is sufficiently long that there is a significant probability that more than one collision with a perturber will occur before radiative decay. In that case, the measurements may be skewed because transitions unlikely to occur in a single step may appear to be enhanced because they arise from a two-step process. Such effects occur in the present experiments carried out in Lyon at low  $v$ , and we have made corrections to our results using the method described in Subsection 3 of the Appendix.

Figure 16 presents comparisons of rate coefficients for each of two transitions with and without consideration of multiple collision effects. Panel (a) shows rate coefficients for NaK  $2(A)^1\Sigma^+(v = 0, J = 14)$  with argon; panel (b) shows rate

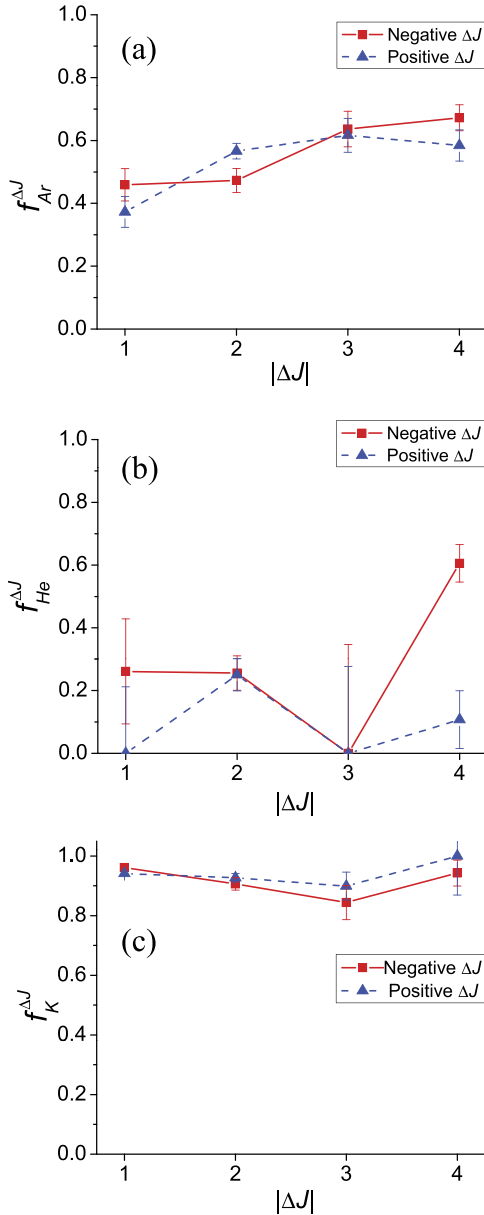


FIG. 14. Experimental values for the fraction of orientation destroyed,  $f_{\text{Ar}}^{\Delta J}$ ,  $f_{\text{He}}^{\Delta J}$ , and  $f_{\text{K}}^{\Delta J}$ , in rotationally inelastic collisions of NaK  $2(A)^1\Sigma^+(v=16, J=30)$  molecules with (a) argon, (b) helium, and (c) potassium atoms as functions of  $\Delta J$ .

coefficients for NaK  $2(A)^1\Sigma^+(v=2, J=44)$  with helium. The effect of the correction is generally to reduce the rates, usually more strongly for larger values of  $|\Delta J|$ . We believe that the actual rate constants lie between the original and “corrected” values but are likely to be closer to the lower corrected values.

#### 4. Spin-orbit effects

Rotationally inelastic collisions of NaK molecules in levels of the  $2(A)^1\Sigma^+$  state can be strongly affected by spin-orbit interactions between specific levels of the  $2(A)^1\Sigma^+$  state and nearby levels of the  $1(b)^3\Pi$  state with the same rotational quantum number  $J$ . In fact, one of the nice features of collisional line spectroscopy is that perturbations can often be identified by quick inspection of the progression of line intensities.

TABLE II. Fraction of orientation destroyed ( $f_p^{\Delta J}$ ) for rotationally inelastic collisions of NaK  $2(A)^1\Sigma^+(v=16, J=30)$  with argon, helium, and potassium atoms ( $p = \text{Ar, He, and K}$ ), and  $g'_p$  values obtained from Eq. (37).

$\Delta J$	$f_{\text{Ar}}^{\Delta J}$	$f_{\text{He}}^{\Delta J}$	$f_{\text{K}}^{\Delta J}$
-4	$0.67 \pm 0.04$	$0.61 \pm 0.06$	$0.94 \pm 0.04$
-3	$0.64 \pm 0.06$	$0.00 \pm 0.35$	$0.84 \pm 0.06$
-2	$0.47 \pm 0.04$	$0.26 \pm 0.05$	$0.91 \pm 0.02$
-1	$0.46 \pm 0.05$	$0.26 \pm 0.17$	$0.96 \pm 0.01$
1	$0.37 \pm 0.05$	$0.00 \pm 0.21$	$0.94 \pm 0.01$
2	$0.57 \pm 0.02$	$0.25 \pm 0.05$	$0.93 \pm 0.01$
3	$0.62 \pm 0.05$	$0.00 \pm 0.28$	$0.90 \pm 0.05$
4	$0.58 \pm 0.05$	$0.11 \pm 0.09$	$1.00 \pm 0.13$
	$g'_{\text{Ar}}$	$g'_{\text{He}}$	$g'_{\text{K}}$
	$(10^{-11} \text{ cm}^3 \text{ s}^{-1})$	$(10^{-11} \text{ cm}^3 \text{ s}^{-1})$	$(10^{-10} \text{ cm}^3 \text{ s}^{-1})$
	3.89 (fixed)	0.56 (fixed)	6.23 (fixed)

It has been well established that collisions are much less likely to induce transitions from an initial  $2(A)^1\Sigma^+$  rovibrational level to a nearby level of the  $1(b)^3\Pi$  state than to another level of the  $2(A)^1\Sigma^+$  state with a similar  $J$  value.<sup>40,41</sup> Presumably this is because singlet  $\rightarrow$  triplet collisional transfer requires a spin flip. As a first approximation, one can assume that singlet  $\rightarrow$  triplet collisional transfer can be neglected compared with transfer within the singlet state. However, spin-orbit interactions between a specific level  $2(A)^1\Sigma^+(v_A, J')$  and a nearby level  $1(b)^3\Pi_{\Omega}(v_b, J')$  with the same rotational quantum number  $J'$  cause the two levels to mix. The result is that the singlet state acquires some triplet character and the triplet state acquires some singlet character.

If the level  $2(A)^1\Sigma^+(v_A, J')$  is perturbed, the rate coefficient for collisions that transfer population from an initial level  $2(A)^1\Sigma^+(v_A, J)$  to the final level  $2(A)^1\Sigma^+(v_A, J' = J + \Delta J)$ , determined directly from experimental line intensities, will be reduced compared with what would be expected in the absence of the perturbation by a factor equal to the square of the singlet state probability amplitude in the mixed final state wave function. In addition,  $2(A)^1\Sigma^+(v_A, J') \rightarrow 1(X)^1\Sigma^+(v_X, J_X = J' \pm 1)$  fluorescence will be further suppressed because the radiative rate is also reduced by the square of the singlet state probability amplitude. Evidence of such perturbations is apparent in the experimental rate coefficients for  $2(A)^1\Sigma^+(v_A = 1, J = 26)$  at  $\Delta J = 6$  and  $\Delta J = 13-15$  shown in Fig. 9. Harker *et al.*<sup>28</sup> found that the level  $2(A)^1\Sigma^+(v_A = 1, J = 32)$  is locally perturbed by  $1(b)^3\Pi_{\Omega=2}(v_b = 5, J = 32)$  such that  $2(A)^1\Sigma^+(v_A = 1, J = 32)$  has only 67% singlet character, while the neighboring levels  $2(A)^1\Sigma^+(v_A = 1, J = 31)$  and  $2(A)^1\Sigma^+(v_A = 1, J = 33)$  are both almost pure singlet (96% and 95% singlet character, respectively). Hence in Fig. 9 we see a strong suppression of the  $\Delta J = +6$  rate coefficients, relative to what we would expect in the absence of perturbation. Similarly, all of the levels  $2(A)^1\Sigma^+(v_A = 1, J = 39-41)$  and  $2(A)^1\Sigma^+(v_A = 1, J = 42-49)$  are significantly perturbed (singlet character  $< 80\%$ ) by the corresponding rotational levels of  $1(b)^3\Pi_{\Omega=1}(v_b = 5)$  and  $1(b)^3\Pi_{\Omega=0}(v_b = 5)$ , respectively, with the strongest perturbations occurring at  $J = 40$  and  $47$  ( $\Delta J = 14$  and  $21$ ,

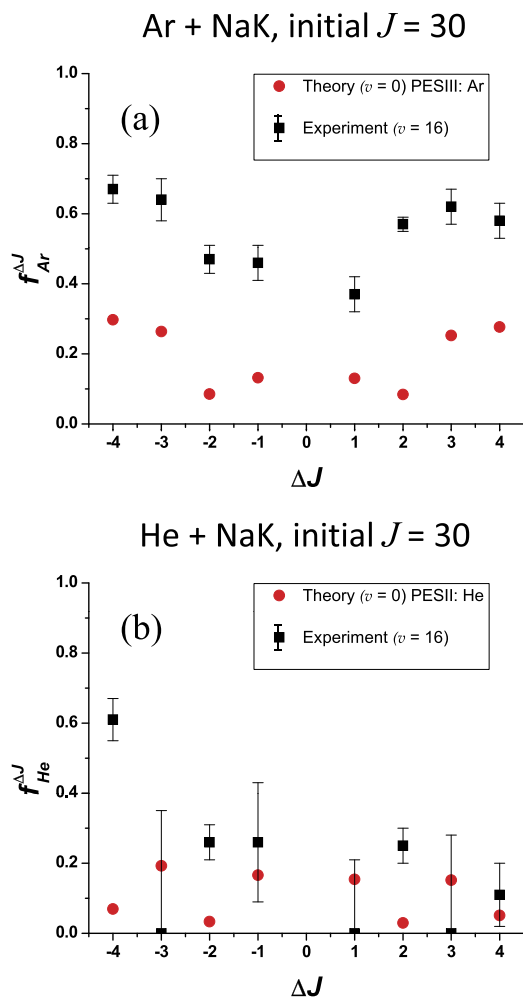


FIG. 15. Comparison between theory and experiment of the fraction of orientation destroyed in rotationally inelastic collisions of NaK  $2(A)^1\Sigma^+$  molecules with (a) argon and (b) helium atoms, as a function of  $\Delta J$ , for initial  $J = 30$ . The codes PES III: Ar and PES II: He in the legends refer to potential energy surfaces calculated in Ref. 21. The experimental data correspond to NaK  $2(A)^1\Sigma^+(v = 16)$ , and the theoretical results correspond to NaK  $2(A)^1\Sigma^+(v = 0)$ .

respectively, in Fig. 9). The suppression of the rate coefficient for  $\Delta J = 14$ , relative to what we would expect in the absence of perturbation, is clearly evident in Fig. 9. The  $v_A = 2$ ,  $J = 27-31$  levels ( $-17 \leq \Delta J \leq -13$ ) are also perturbed, by the corresponding rotational levels of  $1(b)^3\Pi_{\Omega=0}(v_b = 6)$ , with  $J = 29$  ( $\Delta J = -15$ ) being most strongly perturbed. We note that most of the levels studied in this work, specifically  $2(A)^1\Sigma^+(v_A = 0, J \leq 50)$ ,  $2(A)^1\Sigma^+(v_A = 1, J \leq 31)$ , and  $2(A)^1\Sigma^+(v_A = 2, 37 \leq J \leq 60)$  all have singlet character  $>96\%$ , and, therefore, are not significantly affected by perturbations. The NaK  $2(A)^1\Sigma^+(v_A = 16, 26 \leq J \leq 34)$  levels, studied in the OODR experiments at Lehigh, can also be considered to be “pure” singlets ( $>99.6\%$  singlet character).

Incorporating these spin-orbit perturbations into the rate equation analysis of Sec. III A 1 is problematic because perturbed  $2(A)^1\Sigma^+$  levels have lower radiative rates and different collisional rates than unperturbed levels, and this violates our assumption that all neighboring levels have the same quenching and radiative rates. If we assume that the singlet probability amplitude in the perturbed collisional level wave function is

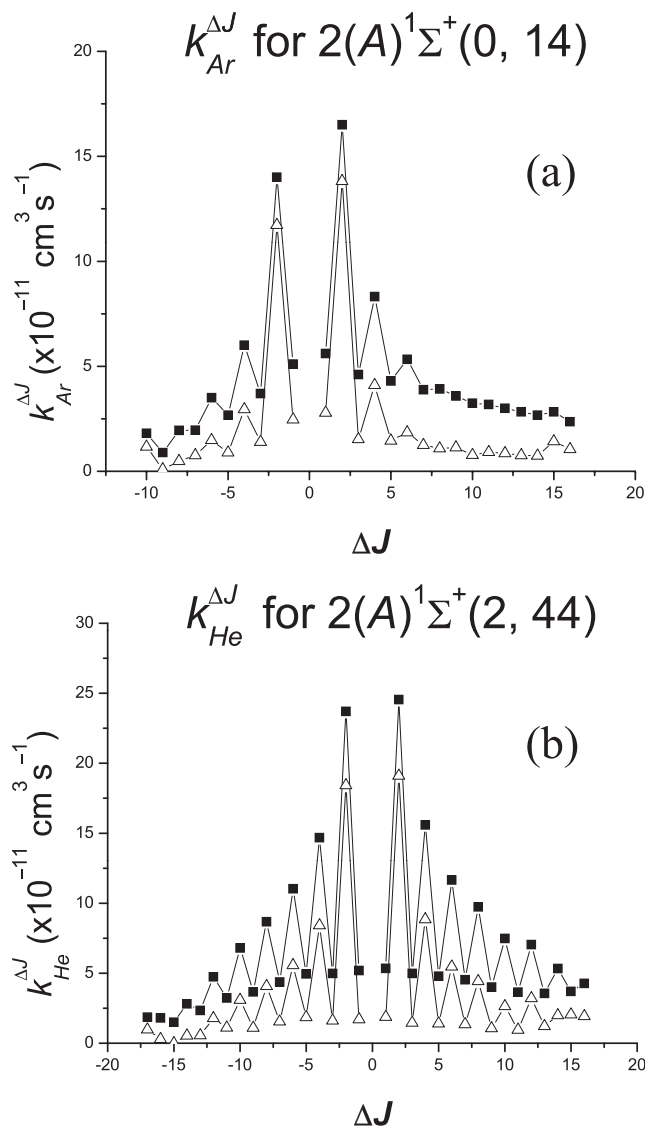


FIG. 16. Comparison of zeroth order (fit neglecting multiple collision effects—solid symbols) and final rate coefficients including multiple collision effects (open symbols) for rotationally inelastic collisions of (a) NaK  $2(A)^1\Sigma^+(v = 0, J = 14)$  molecules with argon and (b) NaK  $2(A)^1\Sigma^+(v = 2, J = 44)$  molecules with helium as functions of  $\Delta J$ . The final values were obtained from the average of the 99th and 100th iterations for (a) and from the average of the 99th and 1000th iterations for (b). See Subsection 3 of the Appendix.

$a$ , then the transition rate  $\Gamma_{C \rightarrow \ell_C}$  associated with the observed fluorescence line intensity  $I_{C \rightarrow \ell_C}$  [see Eqs. (7) and (8)] will be a factor of  $a^2$  weaker than if the level was not perturbed, and hence a factor of  $a^2$  should be introduced on the right-hand side of Eqs. (9) and (11). Assuming that the total radiative rate for levels of the  $1(b)^3\Pi$  state are much smaller than for levels of the  $2(A)^1\Sigma^+$  state, we can assume that each factor of  $\Gamma_C$  in Eqs. (9) and (11) should also be reduced by a factor of  $\sim a^2$  compared with those for unperturbed levels. However, the quenching rate coefficients of perturbed levels should be allowed to vary in the fits, rather than being fixed at the values determined for unperturbed levels. Nevertheless, one might expect  $1(b)^3\Pi$  and  $2(A)^1\Sigma^+$  levels to have quenching rate coefficients that are not too different from each other since rotationally inelastic collisions among  $1(b)^3\Pi$  levels can also

occur and contribute to the perturbed level quenching with a weighting of  $(1 - a^2)$ . Making that assumption therefore suggests that the values of  $k_p^Q/\Gamma_C$  in Eqs. (9) and (11) should be larger than those for unperturbed levels by a factor of  $\sim a^{-2}$  (due to the  $\Gamma_C$  factor). A fit of the  $(v = 1, J = 26) \rightarrow (v = 1, J = 32)$  data [ $\Delta J = +6$  in Fig. 9] with these assumptions results in fitted values  $k_{\text{Ar}}^{\Delta J=+6} = 2.07 \times 10^{-11} \text{ cm}^3 \text{ s}^{-1}$  and  $k_{\text{He}}^{\Delta J=+6} = 6.34 \times 10^{-11} \text{ cm}^3 \text{ s}^{-1}$ . These values are larger than the original fitted values  $k_{\text{Ar}}^{\Delta J=+6} = 1.60 \times 10^{-11} \text{ cm}^3 \text{ s}^{-1}$  and  $k_{\text{He}}^{\Delta J=+6} = 4.78 \times 10^{-11} \text{ cm}^3 \text{ s}^{-1}$  (see Table 11 of the [supplementary material](#)) but less than the expected values (if only the effect of  $\Gamma_{C \rightarrow \ell_C}$  on  $I_{C \rightarrow \ell_C}$  is taken into account) of  $a^{-2}$  times the original fitted values (i.e.,  $2.39 \times 10^{-11} \text{ cm}^3 \text{ s}^{-1}$  and  $7.17 \times 10^{-11} \text{ cm}^3 \text{ s}^{-1}$ , respectively). But these values are still quite a bit less than  $\Delta J = +6$  rate coefficients we would expect based on our measurements with other pump transitions, verifying that the perturbation does indeed significantly reduce the collisional population transfer.

Finally we note that for each perturbed singlet level there is an associated triplet level with substantial singlet character. Collisional population transfer to these levels must also occur. However, we did not investigate collisional transfer to these primarily triplet levels in the present work.

## B. Results for NaCs

As a comparison to the NaK rotationally inelastic collisional population transfer studies, we collected similar data at Lehigh University for collisions of argon perturbers with NaCs molecules that had been excited to the  $2(A)^1\Sigma^+(v = 14, J = 32)$  level. The most significant result of this experiment is that no propensity for  $\Delta J = \text{even}$  transitions is observed for NaCs–Ar collisions. Preliminary data obtained using helium perturbers showed a very slight propensity for  $\Delta J = \text{even}$  collisions.

The NaCs data were fit using Eq. (23) with  $k_{\text{NG}}^{\Delta J, Q} = k_{\text{Ar}}^{\Delta J, Q}$  and  $k_{\text{alk}}^{\Delta J, Q} = k_{\text{Cs}}^{\Delta J, Q}$ . However, the initial fits resulted in non-physical values for the cesium rate coefficients:  $k_{\text{Cs}}^{\Delta J=+1} = 0$  and  $k_{\text{Cs}}^Q$  is very small. We attribute this to the fact that the cesium density was generally low relative to the argon density and hence the data were not sensitive to the cesium rates. Because of this, we carried out a series of fits with  $k_{\text{Cs}}^Q/\Gamma$  fixed at various values over a broad range consistent with our measured NaK potassium quenching rate coefficients,  $k_{\text{K}}^Q/\Gamma$ . With  $k_{\text{Cs}}^Q/\Gamma$  fixed to any value between  $10^{-16} \text{ cm}^3$  and  $10^{-15} \text{ cm}^3$ , we obtain values for  $k_{\text{Cs}}^{\Delta J=+1}$  that are reasonable. In addition, we determined that fixing  $k_{\text{Cs}}^Q/\Gamma$  to any reasonable value and even setting it to zero or letting it vary in the fit has little effect on the argon rate coefficients. Figure 17(a) presents the argon population transfer rate coefficients obtained with various fixed values of  $k_{\text{Cs}}^Q/\Gamma$  or with  $k_{\text{Cs}}^Q/\Gamma$  allowed to vary. The NaCs argon quenching rate coefficient varied between  $(k_{\text{Ar}}^Q/\Gamma) = 2.0\text{--}2.6 \times 10^{-17} \text{ cm}^3$  in these fits. The  $k_{\text{Cs}}^{\Delta J}$  values essentially scale with  $k_{\text{Cs}}^Q$ , and therefore we cannot determine absolute values of the former. However, Fig. 17(b) shows a plot of the values of  $k_{\text{Cs}}^{\Delta J}/k_{\text{Cs}}^Q$  obtained either with different fixed values of  $k_{\text{Cs}}^Q/\Gamma$  or when  $k_{\text{Cs}}^Q/\Gamma$  was allowed to vary. Therefore, this plot shows

relative values of  $k_{\text{Cs}}^{\Delta J}$  (in units of  $k_{\text{Cs}}^Q$ ), and these can be put on an absolute scale if a measured or calculated NaCs–Cs quenching rate coefficient becomes available in the future. Rate coefficients  $k_p^{\Delta J}/\Gamma$  and  $k_p^Q/\Gamma$  obtained in these fits are listed in Tables 25–32 of the [supplementary material](#). Values of  $k_p^{\Delta J}/\Gamma$  and  $k_p^Q/\Gamma$  were converted to rate coefficients  $k_p^{\Delta J}$  and  $k_p^Q$  using  $\Gamma = 2.82 \times 10^7 \text{ s}^{-1}$ , which was determined using LEVEL<sup>34</sup> with the NaCs  $2(A)^1\Sigma^+$  potential of Ref. 42, the  $1(X)^1\Sigma^+$  potential of Ref. 43, and the transition dipole moment of Ref. 44. These  $k_p^{\Delta J}$  values are also listed in Tables 25–32 of the [supplementary material](#). We believe that the most reliable results are those obtained with  $k_{\text{Cs}}^Q/\Gamma$  fixed to the value  $3.0 \times 10^{-16} \text{ cm}^3$  (approximately equal to the value of  $k_{\text{K}}^Q/\Gamma$  obtained in the NaK  $2(A)^1\Sigma^+(v = 16, J = 30)$  experiment at Lehigh), and calculated  $R_F$  values obtained with these parameters are plotted

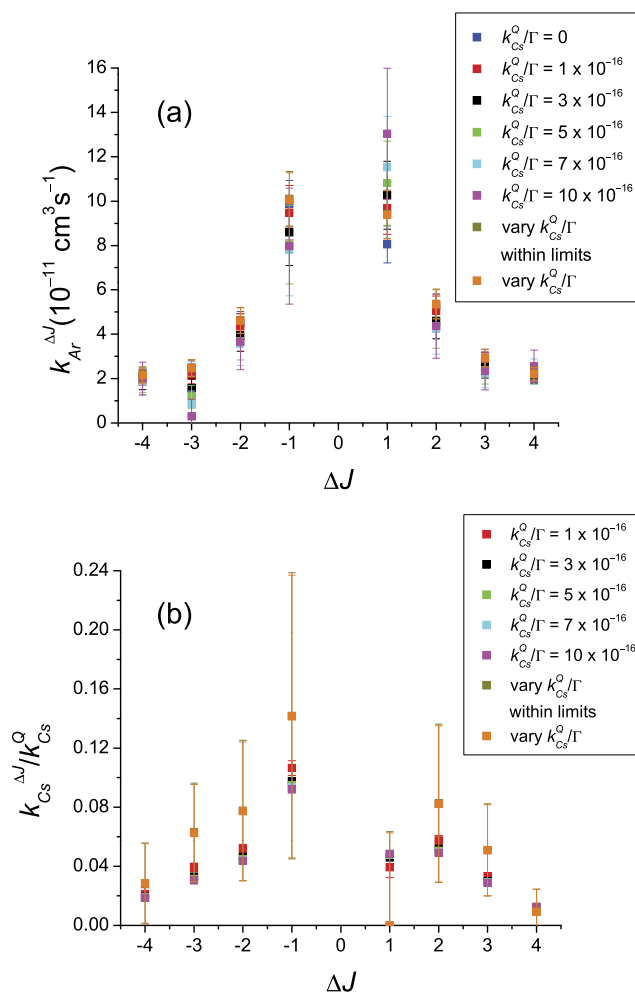


FIG. 17. (a) Rate coefficients  $k_{\text{Ar}}^{\Delta J}$  for rotationally inelastic collisions of NaCs  $2(A)^1\Sigma^+(v = 14, J = 32)$  molecules with argon atoms, comparing the results of fits obtained with various fixed values of  $k_{\text{Cs}}^Q/\Gamma$  or with  $k_{\text{Cs}}^Q/\Gamma$  allowed to vary. (b) Rate coefficients for rotationally inelastic collisions of NaCs  $2(A)^1\Sigma^+(v = 14, J = 32)$  molecules with cesium atoms, in units of the cesium quenching rate coefficient  $k_{\text{Cs}}^Q$ , comparing the results of fits obtained with various fixed values of  $k_{\text{Cs}}^Q/\Gamma$  or with  $k_{\text{Cs}}^Q/\Gamma$  allowed to vary.  $k_{\text{Cs}}^Q/\Gamma$  values are in units of  $\text{cm}^3$ . For cases listed as “vary  $k_{\text{Cs}}^Q/\Gamma$  within limits,” the range of allowed values was  $1 \times 10^{-17} \text{ cm}^3 < k_{\text{Cs}}^Q/\Gamma < 1 \times 10^{-15} \text{ cm}^3$ . The value of  $\Gamma$  was taken to be  $2.82 \times 10^7 \text{ s}^{-1}$ .

against the measured data in Figs. 36–43 of the [supplementary material](#).

Unlike NaK–Ar collisions, the NaCs collisional spectra and fitted parameters show no propensity for  $\Delta J = \text{even}$  collisional transitions. However, the difference between the cesium rate coefficients  $k_{\text{Cs}}^{\Delta J=+1}$  and  $k_{\text{Cs}}^{\Delta J=-1}$  appears to be a real effect and can be seen directly in the spectra recorded at different cesium densities. Figure 44 of the [supplementary material](#) shows two collisional progressions recorded with different cesium densities but similar argon densities. There it can be seen that the ratio  $(k_{\text{Cs}}^{\Delta J=-1}/k_{\text{Cs}}^{\Delta J=+1}) > 1$  in both cases but is significantly larger in the case of higher cesium density implying a fairly strong propensity for  $\Delta J = -1$  over  $\Delta J = +1$  for NaCs–Cs collisions. This is just the opposite of what we observed for potassium collisions with NaK  $2(A)^1\Sigma^+(v = 16, J = 30)$  molecules. We note that the  $\Delta J = \text{negative}$  propensity in NaCs does not seem to extend past  $|\Delta J| = 1$ .

We have recorded some preliminary data to study rotationally inelastic collisions of NaCs  $2(A)^1\Sigma^+(v = 14, J = 32)$  molecules with helium perturbers. NaK–He collisions display a stronger  $\Delta J = \text{even}$  propensity than NaK–Ar collisions, so data were collected to make a similar comparison between NaCs–He and NaCs–Ar collisions. Figure 45 of the [supplementary material](#) shows a collisional spectrum recorded with helium perturbers and low cesium density (and hence low signal-to-noise ratio). Collisional  $|\Delta J| = 2$  line intensities are comparable to, if not larger than, those of the corresponding  $|\Delta J| = 1$  lines. Thus, it appears that the relative number of NaCs  $\Delta J = \text{even}$  collisions compared with  $\Delta J = \text{odd}$  collisions is significantly greater for helium than for argon perturbers. However, further work is clearly needed before definite conclusions can be reached.

## VI. SUMMARY AND CONCLUSIONS

We have investigated rotationally inelastic collisions of excited heteronuclear diatomic molecules with several atomic perturbers. Collisions of NaK  $2(A)^1\Sigma^+$  molecules with helium and argon exhibit a propensity for  $\Delta J = \text{even}$  transitions, and the propensity is stronger for helium than for argon. Collisions of NaCs  $2(A)^1\Sigma^+$  molecules with argon do not show a propensity for  $\Delta J = \text{even}$ , and the propensity in helium collisions is at best very slight.

One might base a simple explanation of these observations on the fact that homonuclear diatomic molecules obey a strict  $\Delta J = \text{even}$  selection rule for rotationally inelastic collisions. Then one could interpret the propensity for  $\Delta J = \text{even}$  in NaK collisions as resulting from the fact that NaK is “almost homonuclear”<sup>38</sup> since sodium and potassium are both alkali atoms with a relatively small difference in mass. This argument explains the much smaller  $\Delta J = \text{even}$  propensities in NaCs, which is “less homonuclear” than NaK (since the difference in mass of sodium and cesium is much greater than that of sodium and potassium), but it breaks down when one considers the details. There are clear differences between the effects of different perturbers, so the degree of the  $\Delta J = \text{even}$  propensity cannot be explained by properties of the molecule alone. Rather, one must consider the deviation of

the atom-diatom potential energy surface (PES) from symmetry under the exchange of Na and K (or Na and Cs).<sup>38</sup> Our calculations support the idea that the degree of the  $\Delta J = \text{even}$  propensity depends on the details of the potential energy surface.

We have investigated<sup>21</sup> how the form of the potential surface affects the  $\Delta J = \text{even}$  propensity by extending the analysis of Ref. 38. We find that a critical factor influencing the strength of the propensity for  $\Delta J = \text{even}$  transitions is the deviation from symmetry of the PES in a particular range of distance of the perturber from the center of mass of the diatomic molecule. Further discussion of this point can be found in Ref. 21 and will appear in a forthcoming paper.

The experiments on NaK have determined rate coefficients  $k_p^{\Delta J}$  as a function of  $\Delta J$  for several different values of the initial level ( $v, J$ ) and perturber  $p$  (argon, helium, or potassium). Generally speaking, for  $J$  in the range 14–44 and for  $v = 0, 1, 2,$  and  $16$ , the measured rate coefficients for  $J \rightarrow J + \Delta J$  depend more strongly on the perturber than on the initial level ( $v, J$ ). The calculations are in good agreement with the absolute magnitude of the experimental rate coefficients for argon and helium and correctly predict that collisions with helium exhibit a more pronounced propensity for  $\Delta J = \text{even}$  transitions. They also confirm the weak dependence of  $k_p^{\Delta J}$  on  $v$  and  $J$  for the measured values. However, the calculations show a stronger dependence as  $J \rightarrow 0$ , and so further experiments to probe this limit would be useful.

For all pump transitions studied in Lyon, the fitted  $k_{\text{K}}^{\Delta J}$  values show strong  $\Delta J = \text{even}$  propensities (see Figs. 27–30 of the [supplementary material](#)). This dependence appears to be inconsistent with the measurements for ( $v = 16, J = 30$ ) carried out at Lehigh. However, the measurements in Lyon primarily focused on the noble gas collisions, so low potassium atom densities were intentionally used. Consequently, it was difficult to accurately extract the relatively small transfer rates due to potassium from the overall rates due to all collisions. Therefore, we believe the rate coefficients for rotationally inelastic collisions of NaK  $2(A)^1\Sigma^+$  molecules with potassium, derived from the data obtained in the Lyon experiment, are less reliable than those obtained in the Lehigh experiment, and hence the former are only reported in the [supplementary material](#). The Lehigh potassium data for ( $v = 16, J = 30$ ) included some observations recorded in the “heat-pipe mode” where the noble gas is excluded from the interaction region and therefore those measurements should directly reflect the effects of potassium collisions only. These results showed no  $\Delta J = \text{even}$  propensity. However, in light of this apparent inconsistency between the potassium results obtained in the two experiments, we believe the question of whether or not a  $\Delta J = \text{even}$  propensity exists for potassium collisions at small  $v$  remains open.

The fractional loss of orientation  $f_p^{\Delta J}$  in collisions of NaK  $2(A)^1\Sigma^+$  molecules with argon, helium, and potassium perturbers has also been measured. For these experiments, the initial level was  $v = 16, J = 30$ . The calculations of  $f_{\text{He}}^{\Delta J}$  are in reasonable agreement with the measurements, while those for  $f_{\text{Ar}}^{\Delta J}$  significantly underestimate the loss of orientation. The calculations predict that both  $f_{\text{Ar}}^{\Delta J}$  and  $f_{\text{He}}^{\Delta J}$  get larger

as  $J$  gets smaller. This result corresponds to the plausible interpretation that a molecule with low  $J$  is more easily disoriented by impact with a perturber than a molecule rotating with greater angular momentum and energy. The calculations also predict that orientation is more likely to be lost if the transition involves an odd  $\Delta J$  instead of an even  $\Delta J$ . Although we did not observe this experimentally in the case of  $v = 16$ ,  $J = 30$ , the calculations predict that the difference is greatest at small  $J$ . Therefore, additional experiments at lower values of the initial  $J$  would be useful to test this prediction.

## SUPPLEMENTARY MATERIAL

See [supplementary material](#) for additional figures and tables related to this work. Figures related to the Lehigh NaK  $2(A)^1\Sigma^+(v = 16, J = 30)$  experiments (Figs. 1–26), the Lyon NaK  $2(A)^1\Sigma^+(v = 0, 1, \text{ and } 2)$  experiments (Figs. 27–34), the NaCs experiments (Figs. 35–45), and the theoretical calculations (Figs. 46–53) are presented. Tables 1–8 correspond to the NaK  $2(A)^1\Sigma^+(v = 16, J = 30)$  experiments at Lehigh, Tables 9–24 are related to the Lyon NaK  $2(A)^1\Sigma^+(v = 0, 1, \text{ and } 2)$  experiments, and Tables 25–32 refer to the NaCs experiments.

## ACKNOWLEDGMENTS

This work was supported by the National Science Foundation under Grant Nos. PHY-0968898 and PHY-1403060 at Lehigh University. Computational facilities at the Texas Advanced Computing Center (TACC) used for this research were supported by NSF through XSEDE resources provided by the XSEDE Science Gateways Program. CNRS (France) gave financial support for the collaboration between the Lyon and Lehigh groups through a PICS award (PICS05972). T.J.P. and A.P.H. thank Professor Heather Jaeger and Dr. Dabhia Talbi for their assistance in selecting the basis sets for the He + NaK and Ar + NaK potential energy surfaces discussed here.

## APPENDIX: RATIONALE FOR APPROXIMATIONS INTRODUCED IN DATA REDUCTION

### 1. Anisotropy factors

In Sec. III A, we stated that the anisotropy factors cancel in the ratio of collisional to direct line fluorescence intensities [Eq. (6)], i.e.,  $F_{C \rightarrow \ell_C} / F_{D \rightarrow \ell_D} \sim 1$ . This argument is based on the fact that we only compare P collisional lines to P direct lines (or R lines to R lines). However, the anisotropy factor is related to polarization and we know that  $J$ -changing collisions reduce orientation and hence tend to depolarize the fluorescence. Therefore, the anisotropy factor for a collisional line is expected to be at least somewhat different from that of the corresponding direct line.

To obtain an estimate of the magnitude of this effect, we follow an argument similar to that given in the work of Chen *et al.*<sup>45</sup> We pump a particular excited level  $2(A)^1\Sigma^+(v_e, J_e)$  from the ground state level  $1(X)^1\Sigma^+(v_g, J_g)$  using a linearly or circularly polarized laser. The populations in the individual

magnetic sublevels  $M_e$  of the level  $2(A)^1\Sigma^+(v_e, J_e)$  are given by

$$n_{v_e, J_e, M_e} \propto \frac{n_{v_g, J_g}}{2J_g + 1} \sum_{M_g} \left| \left\langle \alpha_g, v_g, J_g, M_g \left| \hat{e}_1 \cdot \vec{\mu} \right| \alpha_e, v_e, J_e, M_e \right\rangle \right|^2, \quad (\text{A1})$$

where  $\alpha_{g,e}$  represents all other quantum numbers needed to represent the state,  $\vec{\mu} = e\vec{r}$  is the electric dipole moment operator of the optically active electron, and  $\hat{e}_1$  is the unit vector (which is in general complex) describing the laser polarization. The fluorescence from the anisotropically populated excited state to the final state  $f$  (various rovibrational levels of the ground state) is partially polarized. The intensity of fluorescence polarized along the  $\hat{e}_2$  direction is

$$I_{\hat{e}_2} \propto \sum_{M_f} \sum_{M_e} n_{v_e, J_e, M_e} \left| \left\langle \alpha_e, v_e, J_e, M_e \left| \hat{e}_2 \cdot \vec{\mu} \right| \alpha_f, v_f, J_f, M_f \right\rangle \right|^2. \quad (\text{A2})$$

In the Lyon fluorescence experiment, the laser propagates in the  $\hat{x}$  direction and is linearly polarized in the  $\hat{z}$  direction. Thus  $\hat{e}_1 = \hat{z}$  and  $\hat{e}_1 \cdot \vec{\mu} = \mu_z$ . We assume that the detection direction lies in the  $xz$  plane at an angle  $\theta$  with respect to  $\hat{z}$ . Then we can consider the fluorescence to consist of two components: one part polarized in a plane containing the  $\hat{z}$  axis and one part polarized perpendicular to  $\hat{z}$ . We call these components  $I_{\parallel}$  and  $I_{\perp}$ , respectively. Plugging (A1) into (A2) for  $\hat{e}_2 = \hat{e}_{\perp} = \hat{y}$  and  $\hat{e}_2 = \hat{e}_{\parallel} = \sin\theta\hat{z} - \cos\theta\hat{x}$ , respectively, we find

$$I_{\perp} \propto \frac{n_{v_g, J_g}}{2J_g + 1} \sum_{M_f} \sum_{M_e} \sum_{M_g} \left\{ \left| \left\langle \alpha_g, v_g, J_g, M_g \left| \mu_z \right| \alpha_e, v_e, J_e, M_e \right\rangle \right|^2 \times \left| \left\langle \alpha_e, v_e, J_e, M_e \left| \mu_y \right| \alpha_f, v_f, J_f, M_f \right\rangle \right|^2 \right\} \quad (\text{A3})$$

and

$$I_{\parallel} \propto \frac{n_{v_g, J_g}}{2J_g + 1} \sum_{M_f} \sum_{M_e} \sum_{M_g} \left\{ \left| \left\langle \alpha_g, v_g, J_g, M_g \left| \mu_z \right| \alpha_e, v_e, J_e, M_e \right\rangle \right|^2 \times \left| \left\langle \alpha_e, v_e, J_e, M_e \left| \mu_z \sin\theta - \mu_x \cos\theta \right| \alpha_f, v_f, J_f, M_f \right\rangle \right|^2 \right\}. \quad (\text{A4})$$

The components of the dipole moment operator can be used to construct a spherical tensor operator  $\mu_q^k$  of rank  $k = 1$ :  $\mu_1^1 = -(2)^{-1/2}e(x + iy)$ ,  $\mu_0^1 = ez$ , and  $\mu_{-1}^1 = (2)^{-1/2}e(x - iy)$ . Then, according to Wigner-Eckart theorem<sup>27</sup>

$$\left\langle \alpha, v, J, M \left| \mu_q^1 \right| \alpha', v', J', M' \right\rangle = (-1)^{1+J'-J} \langle J' M', 1q | JM \rangle \times \langle \alpha, v, J \| \vec{\mu} \| \alpha', v', J' \rangle, \quad (\text{A5})$$

where  $\langle J' M', 1q | JM \rangle$  is the Clebsch-Gordan coefficient and  $\langle \alpha, v, J \| \vec{\mu} \| \alpha', v', J' \rangle$  is the reduced matrix element. The square of the reduced matrix element is proportional to the line strength (i.e., the Hönl-London factor) of the  $J \rightarrow J'$  transition,  $\langle \alpha, v, J \| \vec{\mu} \| \alpha', v', J' \rangle \propto S(J, J')$ , which can be calculated from the formulas given by Kovács,<sup>46</sup> and the Clebsch-Gordan coefficient vanishes unless  $q + M' = M$ . Thus the triple sums in Eqs. (A3) and (A4) reduce to single sums over  $M_g = M$ , and

the fluorescence intensities reduce to products of rotational line strengths and the Clebsch-Gordon coefficients,

$$I_{\perp} \propto S(J_g, J_e) S(J_e, J_f) A_{\perp}, \quad (\text{A6})$$

$$I_{\parallel} \propto S(J_g, J_e) S(J_e, J_f) [A_{\parallel} \sin^2 \theta + A_{\perp} \cos^2 \theta] \quad (\text{A7})$$

with

$$A_{\perp} = \frac{1}{2J_g + 1} \sum_M \frac{1}{2} \left\{ \left| \langle J_f M - 1, 1 | J_e M \rangle \right|^2 + \left| \langle J_f M + 1, 1 - 1 | J_e M \rangle \right|^2 \right\} \left| \langle J_e M, 10 | J_g M \rangle \right|^2 \quad (\text{A8})$$

and

$$A_{\parallel} = \frac{1}{2J_g + 1} \sum_M \left| \langle J_f M, 10 | J_e M \rangle \right|^2 \left| \langle J_e M, 10 | J_g M \rangle \right|^2. \quad (\text{A9})$$

We want to compare the total intensity emitted into infinitesimal solid angle  $d\Omega$  at a particular detection angle  $\theta$ ,  $\varphi$  to the total intensity emitted into all angles.

$$\begin{aligned} \frac{I(\theta, \varphi)}{I_{total}} &= \frac{[I_{\perp}(\theta, \varphi) + I_{\parallel}(\theta, \varphi)] d\Omega}{\int_0^{2\pi} d\varphi \int_{-1}^1 [I_{\perp}(\theta, \varphi) + I_{\parallel}(\theta, \varphi)] d(\cos \theta)} \\ &= \frac{[A_{\parallel} \sin^2 \theta + A_{\perp} (1 + \cos^2 \theta)] d\Omega}{\int_0^{2\pi} d\varphi \int_{-1}^1 [A_{\parallel} \sin^2 \theta + A_{\perp} (1 + \cos^2 \theta)] d(\cos \theta)} \\ &= \frac{[A_{\parallel} \sin^2 \theta + A_{\perp} (1 + \cos^2 \theta)] d\Omega}{\frac{8\pi}{3} A_{\parallel} + \frac{16\pi}{3} A_{\perp}}. \end{aligned} \quad (\text{A10})$$

In the Lyon fluorescence experiment, we observe fluorescence emitted into the backward ( $-\hat{x}$ ) direction, so  $\theta = 90^\circ$ . Therefore, the fraction of direct line fluorescence that reaches the detector is

$$\frac{I(\theta, \varphi)}{I_{total}} = \frac{3[A_{\parallel} + A_{\perp}]}{2A_{\parallel} + 4A_{\perp}} \frac{d\Omega}{4\pi}. \quad (\text{A11})$$

The collisional line fluorescence must be somewhat less polarized than the direct line fluorescence. In the worst case, the collisional line fluorescence is completely unpolarized, and in that case, the fraction of collisional line fluorescence reaching the detector is  $d\Omega/4\pi$ . Thus, in the worst case, the ratio of anisotropy factors used in Eq. (6) is given by

$$\frac{F_{C \rightarrow \ell_C}}{F_{D \rightarrow \ell_D}} = \frac{2A_{\parallel} + 4A_{\perp}}{3[A_{\parallel} + A_{\perp}]}. \quad (\text{A12})$$

Formulas for calculating the Clebsch-Gordon coefficients can be found in the work of Zare.<sup>27</sup> We find that Eq. (A12) yields values of  $F_{C \rightarrow \ell_C}/F_{D \rightarrow \ell_D}$  that depend weakly on  $J$  and on the pump/fluorescence combination (i.e., pump a P line, observe a P line in fluorescence; pump P, observe R, etc.). However, all values calculated from Eq. (A12) range between 0.941 and 0.964 for  $J \geq 14$ . Again, these values represent a worst case scenario since in general the collisional lines are not completely depolarized (and for helium collisions are not depolarized much at all). Therefore, we set the anisotropy factor ratios equal to 1 in our analysis but recognize that the error due to this approximation is no more than  $\sim 5\%$ .

Analysis of the Lehigh pump/probe fluorescence experiment, utilizing a circularly polarized pump and a linearly polarized probe, with fluorescence observed in a direction perpendicular to the laser propagation axis, is more complicated

but can be carried out using similar techniques (see also the work of Chen *et al.*<sup>45</sup>). In this case, it can be shown that the resulting factors are again  $\sim 0.95$  for pumping a P or R transition and probing a P or R transition. However, these factors drop to  $\sim 0.85$  for probing a Q transition (in the present work, no Q transitions were used). These are worst case scenarios since the collisional levels maintain some fraction of the initial orientation, whereas these calculations of the anisotropy factors assume complete scrambling of the  $M$  levels in the collision. We also note that neglecting the anisotropy factor (that is, not dividing the collisional rate coefficient by the anisotropy factor) causes a slight underestimation of the rate coefficients. We do not make this correction since these factors only represent an upper limit for the magnitude of the neglected effect. In addition, we will show below that neglect of multiple collision effects results in a significantly larger overestimation of the rate coefficients.

## 2. Sodium density correction

In all of the analysis presented here for the NaK (NaCs) experiments, we approximate all alkali atom collision rates by potassium (cesium) rates, i.e.,

$$\frac{k_{alk}^{\Delta J}}{\Gamma_C} n_{alk} \approx \frac{k_{K(Cs)}^{\Delta J}}{\Gamma_C} [n_K(n_{Cs})], \quad \frac{k_{alk}^Q}{\Gamma_C} n_{alk} \approx \frac{k_{K(Cs)}^Q}{\Gamma_C} [n_K(n_{Cs})]. \quad (\text{A13})$$

According to the Nesmeyanov vapor pressure formulas,<sup>26</sup> the  $K_2$ , NaK, and  $Na_2$  densities in the NaK experiments are small compared with the potassium atomic density and therefore can be safely neglected. However, the sodium density is typically in the range of 5%–12% of the potassium density, according to the Nesmeyanov formulas, for the range of temperatures used in this experiment. Consequently a better approximation for these alkali terms would be

$$\begin{aligned} \frac{k_{alk}^{\Delta J}}{\Gamma_C} n_{alk} &\approx \frac{k_K^{\Delta J}}{\Gamma_C} n_K + \frac{k_{Na}^{\Delta J}}{\Gamma_C} n_{Na} = \frac{k_K^{\Delta J}}{\Gamma_C} n_K \left( 1 + \frac{k_{Na}^{\Delta J} n_{Na}}{k_K^{\Delta J} n_K} \right), \\ \frac{k_{alk}^Q}{\Gamma_C} n_{alk} &\approx \frac{k_K^Q}{\Gamma_C} n_K + \frac{k_{Na}^Q}{\Gamma_C} n_{Na} = \frac{k_K^Q}{\Gamma_C} n_K \left( 1 + \frac{k_{Na}^Q n_{Na}}{k_K^Q n_K} \right). \end{aligned} \quad (\text{A14})$$

It is not possible for us to separately determine sodium and potassium rate coefficients. However, it is reasonable to assume that the sodium and potassium rate coefficients are comparable. Hence if we assume that  $k_{Na}^{\Delta J} \approx k_K^{\Delta J} \equiv k_{alk}^{\Delta J}$  and  $k_{Na}^Q \approx k_K^Q \equiv k_{alk}^Q$ , we see that

$$\frac{k_{alk}^{\Delta J}}{\Gamma_C} n_{alk} \approx \frac{k_K^{\Delta J}}{\Gamma_C} n_K \left( 1 + \frac{n_{Na}}{n_K} \right) \quad (\text{A15})$$

and similarly for the quenching terms. By neglecting the factor in parentheses in (A15) in our analysis (that is, by just using  $n_{alk} \approx n_K$ ), we effectively underestimate the alkali atom density by 5%–12%, which means we effectively overestimate the alkali rate coefficients (reported here as potassium rate coefficients) by 5%–12%. However, the potassium atom densities have much larger uncertainties of 30% and the assumption that  $k_{Na}^{\Delta J} \approx k_K^{\Delta J}$  is fairly crude. So the reported potassium rate coefficients were not corrected for this effect since it

is already taken into account in the error bars. In the NaCs experiment, this effect is considerably less because the ratios  $n_{\text{Na}}/n_{\text{Cs}}$  are much smaller than the  $n_{\text{Na}}/n_{\text{K}}$  ratios in the NaK experiments.

We note that the noble gas rate coefficients are not affected by this systematic underestimation of the alkali atom density.

### 3. Multiple collision corrections

The analysis presented above is based on a “single collision regime” model, where we assume that a particular collisional level  $C$  is much more likely to be populated by a single collision transferring population from the directly excited level (i.e.,  $D \rightarrow C$ ) than it is to be populated through a two (or more) step collisional process involving an intermediate level  $i$ . The benefit of using this approximation,

$$\frac{k_p^{\Delta J}}{\Gamma_C} n_p \gg \sum_{i \neq D} \frac{k_p^{\Delta J_i}}{\Gamma_C} n_p \frac{n_i}{n_D}, \quad (\text{A16})$$

for each perturber  $p$ , is that it allows the neglect of the multiple collision term relative to the single collision term in Eq. (3). This criterion requires both low noble gas atom densities and low alkali atom densities. However, the density of NaK molecules approximately scales with the product of the sodium and potassium atom densities, such that low alkali densities result in greatly reduced direct line intensities. Collisional line intensities are reduced even more than direct line intensities at low noble gas and low alkali densities since each collision rate also scales with the corresponding perturber density. Unfortunately, the perturber densities required for acceptable signal-to-noise put us into the multiple collision regime for some of the data obtained in this work. As will be seen below, this effect is more significant for larger values of  $\Delta J$  and therefore is of particular importance in the interpretation of the data from the Lyon experiment.

Returning to Eq. (3) and considering the Lyon one-laser fluorescence experiment, we see that the collisional level to direct level population ratio is given by

$$\frac{n_C}{n_D} = \frac{\sum_p \left( \frac{k_p^{\Delta J}}{\Gamma_C} n_p + \sum_{i \neq D} \frac{k_p^{\Delta J_i}}{\Gamma_C} n_p \frac{n_i}{n_D} \right)}{1 + \sum_p \frac{k_p^{Q-C}}{\Gamma_C} n_p}, \quad (\text{A17})$$

where the first term in the numerator represents collisions that transfer population from the directly excited level ( $D$ ) to the designated collisional level ( $C$ ) in one step and the second term in the numerator (the sum over  $i \neq D$ ) represents collisions that populate level  $C$  from other levels  $i \neq D$  that were populated from level  $D$ , either directly or indirectly, in previous collisions. The single collision approximation corresponds to neglecting the second term relative to the first. A look at the sums of the fitted  $J$ -changing collision rate coefficients provides one indication that this approximation may not be valid. Specifically, for each type of perturber  $p$ , the sums of the  $J$ -changing collision rate coefficients should be smaller than the corresponding fitted quenching rate coefficient. However, in Table III we see that these sums are, in fact, larger than the corresponding quenching terms, sometimes by more than a

TABLE III. Comparison of fitted quenching rate coefficients with the sums of the  $k_p^{\Delta J}$  values for a given initial level and given perturber  $p$ . These values were obtained using the global fit results for the quenching rate coefficients and zeroth order  $k_p^{D \rightarrow C(0)}$  rate coefficients for  $p = \text{argon, helium, and potassium}$ .

Directly pumped level	$\sum_J k_{\text{Ar}}^{\Delta J}$ ( $\text{cm}^3 \text{s}^{-1}$ )	$\sum_J k_{\text{He}}^{\Delta J}$ ( $\text{cm}^3 \text{s}^{-1}$ )	$\sum_J k_{\text{K}}^{\Delta J}$ ( $\text{cm}^3 \text{s}^{-1}$ )
$2(A)^1\Sigma^+(0, 14)$	$1.18 \times 10^{-9}$	$2.73 \times 10^{-9}$	$3.56 \times 10^{-8}$
$2(A)^1\Sigma^+(0, 30)$	$1.46 \times 10^{-9}$	$2.84 \times 10^{-9}$	$2.71 \times 10^{-8}$
$2(A)^1\Sigma^+(1, 26)$	$1.20 \times 10^{-9}$	$2.40 \times 10^{-9}$	$2.53 \times 10^{-8}$
$2(A)^1\Sigma^+(2, 44)$	$1.20 \times 10^{-9}$	$2.26 \times 10^{-9}$	$1.79 \times 10^{-8}$
$k_p^Q$ ( $\text{cm}^3 \text{s}^{-1}$ )	$8.27 \times 10^{-10}$	$1.39 \times 10^{-9}$	$2.02 \times 10^{-8}$

factor of two. Thus we need to consider how multiple collision effects can be incorporated into the model.

In principle, all measured ( $n_C/n_D$ ) and ( $n_i/n_D$ ) ratios, derived from the intensity ratios, should be fit simultaneously as functions of the various perturber densities. However this procedure requires a prohibitively large fitting matrix. Fits of the  $|\Delta J| \leq 4$  data alone involve 99 fitted parameters, without the inclusion of multiple collision considerations. On the other hand, correcting the rate coefficients for multiple collision effects after the fact is also problematic because the magnitude of the effect depends on the perturber densities. However, we can calculate an upper limit for the magnitude of the error in the various rate coefficients due to neglect of multiple collisions.

We start by noting that the previously determined  $k_p^{\Delta J}$  values are approximately equal for the same  $\Delta J$  but different initial  $J$ . This means we can, for example, approximate  $k_p^{J=28 \rightarrow J=25}$  (where  $\Delta J = -3$ ) for  $v = 0$  (which was not measured) by  $k_p^{J=30 \rightarrow J=27}$  (which was measured). The rate coefficients obtained in our original fit, which we now designate as the zeroth order rate coefficients  $k_p^{\Delta J(0)}$ , in fact represent the sum of the actual rate coefficients for the one-step collisional transfer from the directly excited level ( $k_p^{D \rightarrow C(\text{actual})}$ ) and the actual multiple collision terms that populate level  $C$  from all other levels  $i$ , i.e., ( $k_p^{i \rightarrow C(\text{actual})} \frac{n_i}{n_D}$ ). Thus, for a given perturber, we have

$$k_p^{\Delta J(0)} = \left[ k_p^{D \rightarrow C(\text{actual})} + \sum_{i \neq D} k_p^{i \rightarrow C(\text{actual})} \frac{n_i}{n_D} \right] \quad (\text{A18})$$

or

$$k_p^{\Delta J(\text{actual})} = \left[ k_p^{D \rightarrow C(0)} - \sum_{i \neq D} k_p^{i \rightarrow C(\text{actual})} \frac{n_i}{n_D} \right]. \quad (\text{A19})$$

Here  $k_p^{\Delta J} = k_p^{D \rightarrow C}$  and  $\Delta J = C - D$ . One way to proceed is to use the zeroth order  $k_p^{\Delta J(0)}$  values as estimates of  $k_p^{i \rightarrow C(\text{actual})}$  using  $\Delta J = C - i$ . In principle, using this approximation and known values for ( $n_i/n_D$ ), we can obtain a first order estimate for each  $k_p^{\Delta J(\text{actual})}$ ,

$$k_p^{\Delta J(1)} = \left[ k_p^{D \rightarrow C(0)} - \sum_{i \neq D} k_p^{\Delta J = C - i(0)} \frac{n_i}{n_D} \right]. \quad (\text{A20})$$

This can be iterated such that

$$k_p^{\Delta J(m)} = \left[ k_p^{D \rightarrow C(0)} - \sum_{i \neq D} k_p^{\Delta J=C-i(m-1)} \frac{n_i}{n_D} \right]. \quad (\text{A21})$$

In practice, for high perturber densities, some (or all) of the  $k_p^{\Delta J(1)}$  values turn out to be negative, which implies that effects due to multiple collisions require more than a small correction at these densities. This causes the iteration process to fail because the zeroth order rate coefficients are not a sufficiently good first estimate for the actual rate coefficients. Therefore, we use another method of estimating the first order rate coefficients. Returning to Eq. (A18) we can write

$$\frac{k_p^{D \rightarrow C(\text{actual})}}{k_p^{D \rightarrow C(0)}} = \frac{k_p^{D \rightarrow C(\text{actual})}}{k_p^{D \rightarrow C(\text{actual})} + \sum_{i \neq D} k_p^{i \rightarrow C(\text{actual})} \frac{n_i}{n_D}}, \quad (\text{A22})$$

which is exact. It is not unreasonable to assume, as a first approximation, that each  $\Delta J$  collision is affected equally by multiple collisions, i.e.,  $(k_p^{D \rightarrow C(\text{actual})}/k_p^{D \rightarrow C(0)}) \sim \text{constant}$ . Thus we can form an alternative first approximation to the actual rate coefficients,

$$\frac{k_p^{D \rightarrow C(1)}}{k_p^{D \rightarrow C(0)}} = \frac{k_p^{D \rightarrow C(0)}}{k_p^{D \rightarrow C(0)} + \sum_{i \neq D} k_p^{i \rightarrow C(0)} \frac{n_i}{n_D}}. \quad (\text{A23})$$

These first order estimates can then be iterated to convergence using Eq. (A21).

We carried out this process recognizing that this method is far from exact since the corrections depend on density through the terms  $(n_i/n_D)$ . In fact, because the zeroth order rate coefficients were fit to the density ratios, we can accurately replace  $(n_i/n_D)$  in the equations above with

$$\frac{n_i}{n_D} = \frac{\sum_p \frac{k_p^{D \rightarrow i(0)}}{\Gamma} n_p}{1 + \sum_p \frac{k_p^Q}{\Gamma} n_p}. \quad (\text{A24})$$

Thus the corrected (iterated) rate coefficients would only represent the actual rate coefficients if the perturber densities were the values used in Eq. (A24) for all recorded data. However, by using the highest experimental perturber densities in (A24) and carrying out the calculations outlined above, we obtain a good estimate of an upper limit for the errors in our measured rate coefficients due to neglect of multiple collision effects. In slightly more than half the cases, this process converges to a consistent set of rate coefficients. In the other cases, the iteration process does not converge, but the iterated values oscillate about average values that remain approximately constant. In such cases, we take these average values to be the “corrected” values.

Figure 16 shows the original and “corrected”  $2(A)^1\Sigma^+(0, 14)$  rate coefficients for argon perturbers and  $2(A)^1\Sigma^+(2, 44)$  rate coefficients for helium perturbers, and additional plots and tables for all studied pump transitions and perturbers are provided in Figs. 31–34 and Tables 13–24 of the [supplementary material](#). In all cases, we believe that the actual rate coefficients lie between the original and “corrected” values but are likely

TABLE IV. Comparison of fitted quenching rate coefficients with the sums of the  $k_p^{\Delta J}$  values for a given initial level. These values were obtained using the global fit results for the quenching rate coefficients and the multiple collision analysis results for the  $k_p^{\Delta J}$  rate coefficients.

Directly pumped level	$\sum_J k_{\text{Ar}}^{\Delta J}$ ( $\text{cm}^3 \text{ s}^{-1}$ )	$\sum_J k_{\text{He}}^{\Delta J}$ ( $\text{cm}^3 \text{ s}^{-1}$ )	$\sum_J k_{\text{K}}^{\Delta J}$ ( $\text{cm}^3 \text{ s}^{-1}$ )
$2(A)^1\Sigma^+(0, 14)$	$5.90 \times 10^{-10}$	$1.16 \times 10^{-9}$	$1.80 \times 10^{-8}$
$2(A)^1\Sigma^+(0, 30)$	$6.79 \times 10^{-10}$	$1.14 \times 10^{-9}$	$1.27 \times 10^{-8}$
$2(A)^1\Sigma^+(1, 26)$	$6.22 \times 10^{-10}$	$1.14 \times 10^{-9}$	$1.32 \times 10^{-8}$
$2(A)^1\Sigma^+(2, 44)$	$6.23 \times 10^{-10}$	$1.15 \times 10^{-9}$	$9.31 \times 10^{-9}$
$k_p^Q$ ( $\text{cm}^3 \text{ s}^{-1}$ )	$8.27 \times 10^{-10}$	$1.39 \times 10^{-9}$	$2.02 \times 10^{-8}$

to be closer to the lower corrected values. In Table IV, we see that the sums of these corrected  $k_p^{\Delta J}$  values are now consistent with the fitted quenching rates.

From Fig. 16 of this work and Figs. 31–34 and Tables 13–24 of the [supplementary material](#), it can be seen that the multiple collision effects are relatively small for the largest rate coefficients corresponding to  $|\Delta J| = 2$  but are more significant for small rate coefficients and for large  $|\Delta J|$ . It is also important to note that although these multiple collision corrections have a strong effect on absolute rate coefficients, they have a much smaller effect on *relative* values of rate coefficients for different  $\Delta J$ 's. Specifically, these corrections indicate that the  $\Delta J = \text{even}$  propensity is actually more pronounced than the original fitted values indicate.

Finally, we note that the Lehigh  $2(A)^1\Sigma^+(16, 30)$  data are much less sensitive to multiple collision effects because these data were limited to  $|\Delta J| \leq 4$  and were typically recorded at lower perturber densities. Therefore we do not present such corrections for the Lehigh data.

<sup>1</sup>C. Ottinger, R. Velasco, and R. N. Zare, “Some propensity rules in collision-induced rotational quantum jumps,” *J. Chem. Phys.* **52**, 1636–1643 (1970).

<sup>2</sup>C. Ottinger and D. Poppe, “Collision-induced rotational and vibrational quantum jumps in electronically excited  $\text{Li}_2$ ,” *Chem. Phys. Lett.* **8**, 513–518 (1971).

<sup>3</sup>K. Bergmann and W. Demtröder, “Inelastic collision cross section of excited molecules I. Rotational energy transfer within the  $B^1\Pi_u$ -state of  $\text{Na}_2$  induced by collisions with He,” *Z. Phys.* **243**, 1–13 (1971).

<sup>4</sup>K. Bergmann and W. Demtröder, “Inelastic collision cross section of excited molecules II. Asymmetries in the cross section for rotational transitions in the  $\text{Na}_2(B^1\Pi_u)$  state,” *J. Phys. B: At. Mol. Phys.* **5**, 1386–1395 (1972).

<sup>5</sup>K. Bergmann and W. Demtröder, “Inelastic cross sections of excited molecules III. Absolute cross sections for rotational and vibrational transitions in the  $\text{Na}_2(B^1\Pi_u)$  state,” *J. Phys. B: At. Mol. Phys.* **5**, 2098–2106 (1972).

<sup>6</sup>T. A. Brunner, R. D. Driver, N. Smith, and D. E. Pritchard, “Rotational energy transfer in  $\text{Na}_2^*-\text{Xe}$  collisions: Level to level dynamics,” *J. Chem. Phys.* **70**, 4155–4167 (1979).

<sup>7</sup>T. P. Scott, N. Smith, and D. E. Pritchard, “Application of fitting laws to rotationally inelastic rate constants:  $\text{Li}_2^*(A^1\Sigma) + \text{Ne, Ar, Xe}$ ,” *J. Chem. Phys.* **80**, 4841–4850 (1984).

<sup>8</sup>B. Stewart, P. D. Magill, T. P. Scott, J. Derouard, and D. E. Pritchard, “Quasiresonant vibration  $\leftrightarrow$  rotation transfer in atom-diatom collisions,” *Phys. Rev. Lett.* **60**, 282–285 (1988).

<sup>9</sup>P. D. Magill, B. Stewart, N. Smith, and D. E. Pritchard, “Dynamics of quasiresonant vibration-rotation transfer in atom-diatom scattering,” *Phys. Rev. Lett.* **60**, 1943–1946 (1988).

<sup>10</sup>P. D. Magill, T. P. Scott, N. Smith, and D. E. Pritchard, “Level-to-level vibrationally inelastic rate constants for  $\text{Li}_2^*-\text{X}$  ( $\text{X} = \text{He, Ne, Ar, Xe}$ ) collisions,” *J. Chem. Phys.* **90**, 7195–7206 (1989).

- <sup>11</sup>B. Stewart, P. D. Magill, and D. E. Pritchard, "Quasi-resonant vibration-rotation transfer in inelastic  $\text{Li}_2^*-\text{Ne}$  collisions," *J. Phys. Chem. A* **104**, 10565–10575 (2000).
- <sup>12</sup>A. J. McCaffery, "Quasiresonant vibration-rotation transfer: A kinematic interpretation," *J. Chem. Phys.* **111**, 7697–7700 (1999).
- <sup>13</sup>Y. Gao and B. Stewart, "Comparison of experimental and computed vibrationally inelastic rate constants for  $\text{Li}_2 A^1\Sigma_u^+-\text{Ne}$  collisions," *J. Chem. Phys.* **103**, 860–863 (1995).
- <sup>14</sup>Y. Gao, P. S. Gorgone, S. Davis, E. K. McCall, and B. Stewart, "Dependence of level-resolved energy transfer on initial vibrational level in  $\text{Li}_2 A^1\Sigma_u^+-\text{Ne}$  collisions," *J. Chem. Phys.* **104**, 1415–1426 (1996).
- <sup>15</sup>M. H. Alexander and H.-J. Werner, "Rotationally inelastic collisions of  $\text{Li}_2(A^1\Sigma_u^+)$  with Ne: Fully *ab initio* cross sections and comparison with experiment," *J. Chem. Phys.* **95**, 6524–6535 (1991).
- <sup>16</sup>C. M. Wolfe, S. Ashman, J. Bai, B. Beser, E. H. Ahmed, A. M. Lyyra, and J. Huennekens, "Collisional transfer of population and orientation in NaK," *J. Chem. Phys.* **134**, 174301 (2011).
- <sup>17</sup>R. F. Malenda, "Rotationally inelastic collisions of helium with the NaK molecule," Ph.D. dissertation (Lehigh University, 2012), <http://preserve.lehigh.edu/etd/1302/>.
- <sup>18</sup>R. F. Malenda, T. J. Price, J. Stevens, S. L. Uppalapati, A. Fragale, P. M. Weiser, A. Kuczala, D. Talbi, and A. P. Hickman, "Theoretical calculations of rotationally inelastic collisions of He with NaK( $A^1\Sigma^+$ ): Transfer of population, orientation, and alignment," *J. Chem. Phys.* **142**, 224301 (2015).
- <sup>19</sup>A. M. Arthurs and A. Dalgarno, "The theory of scattering by a rigid rotator," *Proc. R. Soc. A* **256**, 540–551 (1960).
- <sup>20</sup>T. J. Price, A. C. Towne, D. Talbi, and A. P. Hickman, "Semiclassical model for the distribution of final polar angles and  $m'$  states in rotationally inelastic collisions," *Chem. Phys. Lett.* **645**, 180–186 (2016).
- <sup>21</sup>T. J. Price, "Rotationally inelastic collisions of ground-state helium or argon with NaK ( $A^1\Sigma^+$ )," Ph.D. dissertation (Lehigh University, 2017), <http://preserve.lehigh.edu/etd/2770/>.
- <sup>22</sup>K. M. Richter, "Studies of rotationally and vibrationally inelastic collisions of NaK with atomic perturbers," Ph.D. dissertation (Lehigh University, 2016), <http://preserve.lehigh.edu/etd/2781/>.
- <sup>23</sup>C. R. Vidal and J. Cooper, "Heat-pipe oven: A new, well-defined metal vapor device for spectroscopic measurements," *J. Appl. Phys.* **40**, 3370–3374 (1969).
- <sup>24</sup>C. G. Carrington, D. N. Stacey, and J. Cooper, "Multipole relaxation and transfer rates in the impact approximation: Application to the resonance interaction," *J. Phys. B: At. Mol. Phys.* **6**, 417–432 (1973).
- <sup>25</sup>N. Lwin and D. McCartan, "Collision broadening of the potassium resonance lines by noble gases," *J. Phys. B: At. Mol. Phys.* **11**, 3841–3849 (1978).
- <sup>26</sup>A. N. Nesmeyanov, *Vapor Pressure of the Elements* (Academic Press, New York, 1963).
- <sup>27</sup>R. N. Zare, *Angular Momentum* (John Wiley & Sons, New York, 1988).
- <sup>28</sup>H. Harker, P. Crozet, A. J. Ross, K. Richter, J. Jones, C. Faust, J. Huennekens, A. V. Stolyarov, H. Salami, and T. Bergeman, "Experimental and theoretical studies of the coupled  $A^1\Sigma^+$  and  $b^3\Pi$  states of NaK," *Phys. Rev. A* **92**, 012506 (2015).
- <sup>29</sup>G. Herzberg, *Molecular Spectra and Molecular Structure I. Spectra of Diatomic Molecules* (Van Nostrand Reinhold, New York, 1950).
- <sup>30</sup>W. Demtröder, *Laser Spectroscopy Volume 2: Experimental Techniques*, 4th ed. (Springer, Berlin, Germany, 2008), pp. 104–117.
- <sup>31</sup>J. A. Jones, "Studies of inelastic collisions of NaK and NaCs molecules with atomic perturbers," Ph.D. dissertation (Lehigh University, 2015), <http://preserve.lehigh.edu/etd/1710/>.
- <sup>32</sup>C. Wolfe, "Collisional transfer of population and orientation in NaK," Ph.D. dissertation (Lehigh University, 2010), <http://search.proquest.com/docview/756252376>.
- <sup>33</sup>E. H. Ahmed, private communication (2017).
- <sup>34</sup>R. J. Le Roy, "LEVEL: A computer program for solving the radial Schrödinger equation for bound and quasibound levels," *J. Quant. Spectrosc. Radiat. Transfer* **186**, 167–178 (2017).
- <sup>35</sup>A. Gerdes, M. Hobein, H. Knöckel, and E. Tiemann, "Ground state potentials of the NaK molecule," *Eur. Phys. J. D* **49**, 67–73 (2008).
- <sup>36</sup>A pointwise version of  $V(R)$  mesh points for the  $1(X)^1\Sigma^+$  state from Ref. 35 was provided by E. Tiemann, private communication (2012).
- <sup>37</sup>S. Magnier, M. Aubert-Frécon, and Ph. Millié, "Potential energies, permanent and transition dipole moments for numerous electronic excited states of NaK," *J. Mol. Spectrosc.* **200**, 96–103 (2000).
- <sup>38</sup>C. W. McCurdy and W. H. Miller, "Interference effects in rotational state distributions: Propensity and inverse propensity," *J. Chem. Phys.* **67**, 463–468 (1977).
- <sup>39</sup>T. J. Price and A. P. Hickman, "Semiclassical analysis of  $jm \rightarrow j'm'$  transitions in rotationally inelastic collisions in a cell," *J. Chem. Phys.* (submitted).
- <sup>40</sup>L. Li, Q. Zhu, A. M. Lyyra, T.-J. Whang, W. C. Stwalley, R. W. Field, and M. H. Alexander, "Collision-induced transitions between  $A^1\Sigma_u^+$  and  $b^3\Pi_u$  states of  $\text{Na}_2$ : The 'gateway' effect of perturbed levels," *J. Chem. Phys.* **97**, 8835–8841 (1992).
- <sup>41</sup>L. Li, S. Antonova, A. Yiannopoulou, K. Urbanski, and A. M. Lyyra, "State-to-state collision energy transfer of  $^7\text{Li}_2$  within high-lying triplet states: Gateway effect of mixed levels in energy transfer between singlet and triplet states," *J. Chem. Phys.* **105**, 9859–9863 (1996).
- <sup>42</sup>J. Zaharova, M. Tamanis, R. Ferber, A. N. Drozdova, E. A. Pazyuk, and A. V. Stolyarov, "Solution of the fully-mixed state problem: Direct deperurbation analysis of the  $A^1\Sigma^+-b^3\Pi$  complex in a NaCs dimer," *Phys. Rev. A* **79**, 012508 (2009).
- <sup>43</sup>O. Docenko, M. Tamanis, R. Ferber, A. Pashov, H. Knöckel, and E. Tiemann, "Spectroscopic studies of NaCs for the ground state asymptote of Na + Cs pairs," *Eur. Phys. J. D* **31**, 205–211 (2004).
- <sup>44</sup>M. Aymar and O. Dulieu, "Calculations of transition and permanent dipole moments of heteronuclear alkali dimers NaK, NaRb and NaCs," *Mol. Phys.* **105**, 1733–1742 (2007).
- <sup>45</sup>H. Chen, L. Li, G. Lazarov, X. Wang, A. M. Lyyra, J. Huennekens, and R. W. Field, "Rotational pattern difference in resolved fluorescence spectra with different detection schemes," *J. Mol. Spectrosc.* **196**, 197–211 (1999).
- <sup>46</sup>I. Kovács, *Rotational Structure in the Spectra of Diatomic Molecules* (American Elsevier, New York, 1969).